

Implication of the Weizsacker-Williams approximation for the dark matter mediator production

I. V. Voronchikhin^{1,*} and D. V. Kirpichnikov^{2,†}

¹*Tomsk Polytechnic University, 634050 Tomsk, Russia*

²*Institute for Nuclear Research, 117312 Moscow, Russia*

The simplified connection between Standard Model (SM) particles and light dark matter (LDM) can be introduced via spin-0 and spin-1 lepton-specific mediators. Moreover, in a mediator mass range from sub-MeV to sub-GeV, fixed-target facilities such as NA64e, LDMX, NA64μ, and M³ can potentially probe such particles of the hidden sector via missing energy signatures that are described by the bremsstrahlung-like process involving leptons. We compare the Weizsacker-Williams (WW) approximation and the exact tree-level (ETL) approach for the bremsstrahlung-like mediator production cross section by choosing various parameters of the fixed-target experiments. We show that the relative difference between the total cross sections calculated in the WW and ETL approximation varies from $\mathcal{O}(1)$ % to $\mathcal{O}(10)$ % for a muon mode and from $\mathcal{O}(-20)$ % to $\mathcal{O}(80)$ % for an electron mode. We argue that the main difference between two approaches for electron beam mode arises from peak forward region of the cross section. We also discuss the impact of parametrization of nuclear and atomic elastic form-factors on the total cross section. In particular, we show that the employing different form-factor parametrization can lead to an uncertainty in the cross section at the level of $\lesssim \mathcal{O}(10)$ %. That study may be helpful for the lepton fixed-target experiments that examine the bremsstrahlung-like production of the DM mediators.

I. INTRODUCTION

Over the past few decades, astrophysical observations lead to the concept of dark matter (DM), which may manifest itself through the gravitational effects [1, 2]. The evidences of the DM imply the galaxy rotation velocities, the cosmic microwave background anisotropy, the gravitational lensing, etc [3–5]. About $\simeq 85\%$ of total mass content in our Universe is associated with the DM which cannot be explained by the Standard Model (SM) [6, 7]. Some scenarios address the DM as a solution for the anomalous magnetic moment puzzle [8], the large-scale structures [9], etc.

Thermal contact between light dark matter (LDM) and SM particles can lead to overproduction of DM particles in the early Universe; therefore, the relic abundance requires a depletion mechanism to yield the observed value [10–12]. To avoid the LDM overproduction one can introduce the scenario with the mediator of DM (MED) that can connect LDM and SM particles via portals. For instance, the typical scenarios and the regarding thermal target associated with dark boson mediators include spin-0, spin-1 and spin-2 particles such as the hidden Higgs boson [13–19], the dark photon [20–31], and the dark graviton [32–43], respectively.

The detection of the DM particles at the accelerator-based experiments is one of a great interest of modern physics. We note that the above-mentioned portal scenarios for LDM provide specific experimental missing energy signatures. Such processes are associated with energy fraction of the primary beam of the charged lepton $l^\pm = (e^\pm, \mu^\pm)$ that can be carried away by the

produced mediator in the bremsstrahlung-like process $l^\pm N \rightarrow l^\pm N + \text{MED}$, followed by invisible decay into pair of DM particles $\text{MED} \rightarrow \chi\chi$. The fixed-target experiments combine the advantages of high-energy particle beam of l^\pm and its relative large intensity in order to probe LDM in the sub-GeV mass range. In particular, as a lepton fixed-target experiments, one can exploit the existing (NA64e [44–56] and NA64μ [57–59]) and the projected (Light Dark Matter Experiment (LDMX) [60–63] and M³ [64, 65]) facilities.

One can exploit the Weizsacker-Williams (WW) approximation [66–68] in order to describe the bremsstrahlung-like production of mediator where the charged high-energy lepton impinging on an active target. Next, the WW method was adapted to bremsstrahlung-like production in the cases of the one-photon exchange process [69, 70] and the photon-fusion process [71]. In general, the WW approximation reduces the integral over momenta space and implies that energy of incoming particle is much greater than the particle masses [69], that simplifies the calculation. The examination of the WW approximation is performed for (i) an electron mode in case of E137 experiments [72, 73], (ii) a muon mode in case of NA64μ [19, 58], and (iii) a proton bremsstrahlung [74–80].

We emphasize that implication of the exact tree-level (ETL) method [81] for a bremsstrahlung-like production of the hidden particles is also widely discussed in the literature for (i) the muon-philic signature [82, 83], (ii) the lepton-flavour-violating process [84–86], accelerator based signatures [53, 54], and (iii) the hidden vector production at electron-ion colliders [87]. However, the study of both WW and ETL methods can also be relevant for accurate bremsstrahlung-like signal calculation at (i) International Linear Collider beam-dump experiments [88, 89], (ii) electron beam-dump experi-

* e-mail: i.v.voronchikhin@gmail.com

† e-mail: dmbriick@gmail.com

ments [90–93], (iii) Belle II experiment [94, 95] (that also exploits bremsstrahlung-like signatures), and (iv) muon beam-dump experiments [96–100].

The WW approximation for the bremsstrahlung-like radiation of mediators has a lot of parameters that can impact the accuracy of calculations. In particular, the accuracy of the cross section calculation can depend on the parameters of the target material, the particle primary beam and its energy, the type of the mediator, and the parametrization of the form-factor. In addition, we note that rate of the DM mediator production is sensitive to the maximum angle of its emission, and the latter can be associated with the specific design and acceptance of the fixed-target facility [72, 73]. As a result, the cut on the emission angle can impact the accuracy of the WW approach for some specific parameter space. We note however, that the implication of the mediator emission angle cut for the cross section accuracy calculation was addressed in Ref. [75], implying the proton-proton collision.

In this paper, we study the implication of the WW approximation for calculating the cross section of different mediator production in various lepton fixed-target experiments. In particular, we continue the study of authors in Refs. [19, 58, 72, 73, 101] and calculate the production cross sections using the ETL and WW methods for scalar, pseudoscalar, vector and axial-vector mediators of SM in the case of NA64e, NA64 μ , LDMX, and M³ experiments. Also, we compare calculations of the total and differential cross sections using the ETL and WW methods for different maximum emission angles of the MED. Additionally, we consider the impact of various form-factors on the cross section calculated in the WW approximation for the specific MED. The latter can be crucial for the bremsstrahlung-like signal estimate, since various atomic form-factor parametrizations are addressed in the literature [73, 87, 102].

The paper is organized as follows. In Sec. II we provide models of mediators and main parameters of the considered lepton fixed-target experiments. In Sec. III we describe the procedure of cross section calculation in the case of bremsstrahlung-like production of mediator at lepton fixed-target experiments. In Sec. IV we discuss the differential and total cross sections for different types of mediator models and lepton fixed-target experiments. In this section we also calculate the total cross sections with corresponding missing energy signatures. We conclude in Sec. V. We collect some helpful formulas in Appendices.

II. BENCHMARK SCENARIOS AND EXPERIMENTS

Let us consider now the simplified lepton-specific interaction with a light scalar, pseudoscalar, vector and axial-vector mediators of DM in the following [72, 73]

$$\mathcal{L}_{\text{eff}}^{\phi} \supset c_{ll}^{\phi} \phi \bar{l} l, \quad (1)$$

$$\mathcal{L}_{\text{eff}}^{\text{P}} \supset c_{ll}^{\text{P}} P \bar{l} \gamma_5 l, \quad (2)$$

$$\mathcal{L}_{\text{eff}}^{\text{V}} \supset c_{ll}^{\text{V}} V^{\mu} \bar{l} \gamma_{\mu} l, \quad (3)$$

$$\mathcal{L}_{\text{eff}}^{\text{A}} \supset c_{ll}^{\text{A}} A^{\mu} \bar{l} \gamma_5 \gamma_{\mu} l, \quad (4)$$

where c_{ll}^{MED} is the dimensionless coupling of lepton with different mediators. In particular, the low-energy Lagrangian for spin-0 mediator can be originated from the flavor-specific five-dimensional effective operator [60, 82, 103–105].

The NA64e experiment is located at the Super Proton Synchrotron (SPS) of the European Organization for Nuclear Research (CERN). Protons from the SPS hitting a beryllium target with a thin lead convector produce a beam of ultra-relativistic electrons, which is scattered by the nuclei of the experiment’s active thick target [46]. The NA64 μ experiment corresponds to the muon beam mode at the M2 line of the SPS in the north area of CERN SPS, which uses the detector system structure of the NA64e experiment. However, in the NA64 μ experiment, an accurate reconstruction of the momentum of the incident particle is important to suppress the background processes [59]. LDMX is a planned electron beam experiment at Stanford Linear Accelerator Center (SLAC) in which missing energy signatures are complemented by a unique technique to measure the missing momentum of electrons [106, 107]. Muon Missing Momentum Experiment (M³) is a muon mode experiment that is developed at SLAC. The M³ experiment is considered as a complementary part of the LDMX and has a similar detector base [63]. In Table. I the parameters of the considered experiments are shown. In addition, the cut for the mediator energy ratio $x_{\text{cut}} = E_{\text{MED}}^{\text{cut}}/E_l$ is used in order to specify the typical missing energy cuts for the MED production cross section in the considered experiments. Note that the total cross section of bremsstrahlung-like MED production for the specific experiment is

$$\sigma_{\text{tot}} = \int_{x_{\text{cut}}}^1 dx \int_0^{\theta_{\text{max}}} d\theta_{\text{MED}} \frac{d\sigma_{2 \rightarrow 3}}{dx d\theta_{\text{MED}}},$$

where the double differential cross section is calculated in Sec. III below for various approaches and θ_{MED} is an angle between initial beam direction and momentum of the produced MED.

III. BREMSSTRAHLUNG-LIKE PRODUCTION OF MEDIATOR

The radiation of a dark matter mediator by a lepton scattering off a heavy nucleus can be represented as a $2 \rightarrow 3$ process as:

$$l^{\pm}(p) + N(P_i) \rightarrow l^{\pm}(p') + N(P_f) + \text{MED}(k), \quad (5)$$

where $p = (E_l, \mathbf{p})$, $p' = (E'_l, \mathbf{p}')$ - momenta of the incoming and outgoing leptons, respectively, $k = (E_{\text{MED}}, \mathbf{k})$ - momentum of the dark matter mediator, $P_i = (M, 0)$ and $P_f = (P_f^0, \mathbf{P}_f)$ - momenta of the

initial and final nucleus, respectively, $q = (q_0, \mathbf{q}) \equiv P_i - P_f$ - momentum transferred to the nucleus. We define the virtuality of the photon in the following form:

$$t \equiv -q^2 = -(P_i - P_f)^2 = 2M \left(\sqrt{M^2 + P_f^2} - M \right) > 0.$$

The Mandelstam-like variables for the process (5) can be introduced as:

$$\begin{aligned} \tilde{s} &= (p' + k)^2 - m_l^2, & \tilde{u} &= (p - k)^2 - m_l^2, \\ \tilde{t} &= (p - p')^2 - m_{\text{MED}}^2, \end{aligned} \quad (6)$$

Also, for the introduced Mandelstam-like variables the expression $\tilde{s} + \tilde{u} + \tilde{t} = -t$ is performed. Using conditions on the mass shell for the outgoing lepton and heavy nucleus in the form $p' = m_l^2$ and $P_f = M^2$, one can obtain:

$$\begin{aligned} q_0 &= -t/(2M), & |\mathbf{q}|^2 &= t^2/(4M^2) + t, \\ t &= 2M(\sqrt{M^2 + |\mathbf{q}|^2} - M) \simeq |\mathbf{q}|^2, \end{aligned} \quad (7)$$

where we take into account that $|\mathbf{q}| \lesssim \mathcal{O}(100)$ MeV and $M \propto \mathcal{O}(100)$ GeV, i.e. the relation $|\mathbf{q}|/M \ll 1$.

In general, the interaction of an electromagnetic field A_μ and a hadron can be effectively represented as [108]:

$$\mathcal{L}_{\text{eff}}^{\text{nuc}} \supset -eA_\mu \mathcal{J}^\mu, \quad (8)$$

where \mathcal{J}^μ is a hadronic current [109, 110]. For a heavy nucleus, one can exploit a spin-0 boson form-factor with a good accuracy [111]. Finally, the hadronic current reads as follows in the momentum space [112, 113]:

$$\mathcal{J}^\mu = F_s(t)(P_f + P_i)^\mu, \quad (9)$$

where $F_s(t)$ - is form-factor, which takes into account the impact of the internal structure through the spatial charge distribution.

The matrix element for the process $2 \rightarrow 3$ can be written as:

$$i\mathcal{M}_{2 \rightarrow 3}^{\text{MED}} = ic_{ll}^{\text{MED}} e^2 \mathcal{L}^\mu \left(\frac{-i\eta_{\mu\nu}}{q^2} \right) \mathcal{J}^\nu. \quad (10)$$

For the lepton current with the radiation of spin-0 or spin-1 mediators, one can get:

$$\begin{aligned} \mathcal{L}^\mu &= \bar{u}(p') \left(\gamma^\mu \frac{\gamma_\sigma (p - k)^\sigma + m_l}{\tilde{u}} C_{\mathcal{L}}^{\text{MED}} + \right. \\ &\quad \left. + C_{\mathcal{L}}^{\text{MED}} \frac{\gamma_\sigma (p' + k)^\sigma + m_l}{\tilde{s}} \gamma^\mu \right) u(p), \end{aligned} \quad (11)$$

where $C_{\mathcal{L}}^{\text{MED}}$ is a typical term for scalar, pseudoscalar, vector and axial mediators, that take the forms, respectively:

$$C_{\mathcal{L}}^{\text{S}} = 1, \quad C_{\mathcal{L}}^{\text{P}} = i\gamma_5, \quad C_{\mathcal{L}}^{\text{V}} = \varepsilon_\nu^*(k)\gamma^\nu, \quad C_{\mathcal{L}}^{\text{A}} = \varepsilon_\nu^*(k)\gamma_5\gamma^\nu,$$

where $\varepsilon_\mu(k)$ is a polarization vector for spin-1 boson.

The nuclear form-factor in the laboratory frame is associated with charge density of nucleus through the Fourier transformation in the case of heavy nuclei [58, 70, 102]. In addition, the atomic form-factor can be represented as the nuclear form-factor with screening by the Coulomb field of atomic electrons. Indeed, the nuclear and atomic

form-factors tend to $F_{\text{nuc}}(t) \rightarrow 1$ and $F_{\text{atom}}(t) \rightarrow 0$ as $t \rightarrow 0$, respectively. Moreover, one can represent screening by the Coulomb field of atomic electrons as a convolution of the nuclear charge density with the specific screening density.

As a result, the nuclear form-factor being multiplied by the screening term yields an atomic form-factor [114]:

$$F_{\text{nuc}}(t) \rightarrow F_{\text{atom}}(t) \equiv F_{\text{scr}}(t)F_{\text{nuc}}(t),$$

$$F_{\text{scr}}(t) = t/(t_a + t),$$

where $\sqrt{t_a} = 1/R_a$ and R_a is typical magnitude of the atomic radius $R_a = 111Z^{-1/3}/m_e$. It is also worth noting that a complete screening regime arises for $t/t_a \ll 1$, implying that the typical atomic form-factor is sufficiently small $F_{\text{atom}}(t) \ll 1$. We note that the virtual photon flux for the inelastic form-factor is proportional to $\propto Z$; thus, this contribution can be omitted in the calculation for heavy nuclei [19, 58, 102].

The elastic atomic Tsai-Schiff's [70, 115], Helm's [116, 117] and exponential [118] form-factors take the following forms, respectively:

$$F_{\text{TS}}(t) = F_{\text{scr}}(t) \frac{1}{(1 + t/t_d)}, \quad (12)$$

$$F_{\text{H}}(t) = F_{\text{scr}}(t) \frac{3j_1(\sqrt{t}R_{\text{H}})}{\sqrt{t}R_{\text{H}}} \exp(-s_{\text{H}}^2 t/2), \quad (13)$$

$$F_{\text{E}}(t) = F_{\text{scr}}(t) \exp(-tR_{\text{exp}}^2/6), \quad (14)$$

where $\sqrt{t_d} = 1/R_n$ is the typical momentum associated with nuclear radius, $s_{\text{H}} = 0.9$ fm is the nuclear shell thickness, the Tsai-Schiff's, Helm's and exponential parametrizations of effective nuclear radius can be written as:

$$R_n \simeq 1/\sqrt{0.164A^{-2/3}\text{GeV}^2}, \quad (15)$$

$$R_{\text{exp}} = (0.91A^{1/3} + 0.3)\text{fm}, \quad (16)$$

$$R_{\text{H}} = \sqrt{c_{\text{H}}^2 + 7/3\pi^2 a_{\text{H}}^2 - 5s_{\text{H}}^2}, \quad (17)$$

$a_{\text{H}} = 0.52$ fm and $c_{\text{H}} = (1.23A^{1/3} - 0.6)$ fm. One can set Helm's form-factors to zero for $t \gtrsim (4.49/R_{\text{H}})^2 \equiv t_{\text{H}}$ due to negative values [117] and also use the notation $t_{\text{exp}} = 1/R_{\text{exp}}^2$. Moreover, for the nucleus of interest the following inequalities hold

$$t_a < t_{\text{H}} < t_{\text{exp}} < t_d.$$

As shown in Appendix A, the ETL double-differential cross section for the bremsstrahlung-like production of the mediator takes the form [72, 73]:

$$\begin{aligned} \frac{d\sigma_{2 \rightarrow 3}}{dx d\cos(\theta_{\text{MED}})} &= \frac{(c_{ll}^{\text{MED}})^2 \alpha^3 Z^2}{4\pi} \frac{|\mathbf{k}|E_p}{|\mathbf{P}||\mathbf{k} - \mathbf{p}|} \\ &\cdot \int_{t_{\text{min}}}^{t_{\text{max}}} dt \frac{F^2(t)}{t^2} \frac{1}{8M^2} \int_0^{2\pi} \frac{d\phi}{2\pi} |\mathcal{A}_{2 \rightarrow 3}^{\text{MED}}|^2, \end{aligned} \quad (18)$$

where $t_{\text{max}}, t_{\text{min}}$ are the maximum and minimum squares of the 4-momentum transferred to the nucleus (A11),

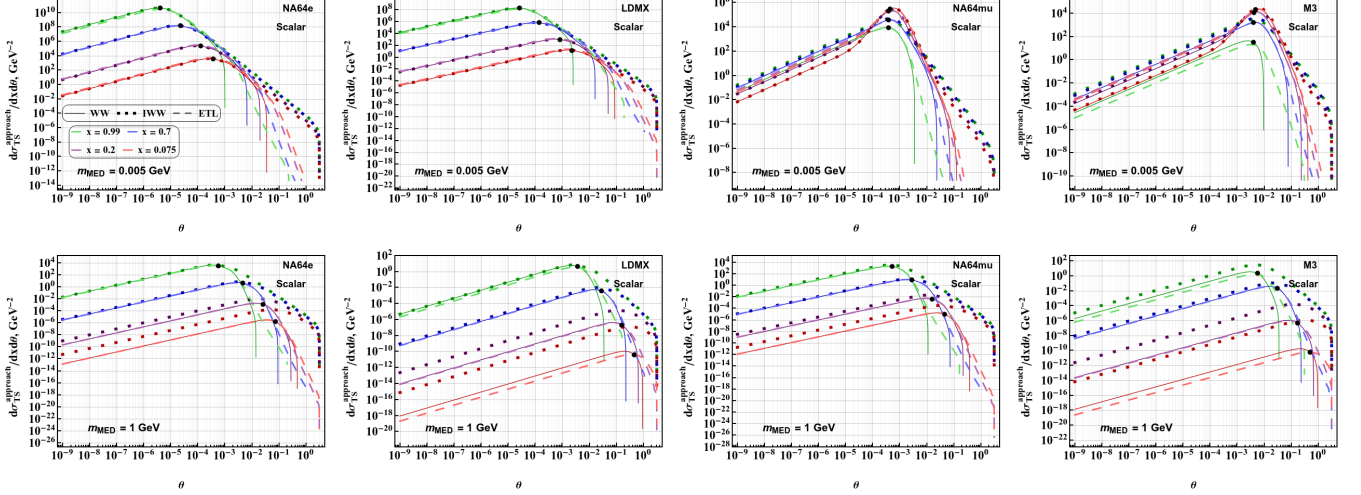


FIG. 1. The double-differential cross section with respect to the emission angle of the scalar mediator $\theta \equiv \theta_\phi$ and its fraction of energy x as a function of θ . Each color in the figures corresponds to a fixed value of fraction of energy x . The solid, dotted and dashed lines correspond to the calculations which exploit the WW, IWW and ETL approaches, respectively. The typical angle of mediator radiation (C4) for the each fixed value of fraction of energy x in the figures are shown by a black point.

	NA64e	LDMX	NA64μ	M ³
target material	Pb	Al	Pb	W
Z , atomic number	82	13	82	74
A , g · mole ⁻¹	207	27	207	184
$x_{\text{cut}} = E_{\text{MED}}^{\text{cut}}/E_l$	0.5	0.7	0.5	0.4
l^\pm , primary beam	electron	electron	muon	muon
E_l , GeV, beam energy	100	16	160	15

TABLE I. The benchmark parameters for the total MED production cross section $l^\pm N \rightarrow l^\pm N + \text{MED}$ at the lepton fixed-target experiments. Note that the $E_{\text{MED}}^{\text{cut}} = x_{\text{cut}} E_l$ is a typical minimum missing energy threshold that is associated with the specific fixed-target facility.

$x = E_{\text{MED}}/E_l$ is the fraction of the total energy of the mediator with respect to the energy of original lepton, and $|\mathcal{A}_{2 \rightarrow 3}^{\text{MED}}|^2$ is mediator production amplitude squared. In addition, the explicit forms of the squared amplitudes for the mediators are given in (A14) - (A17).

Also, the double-differential cross section in the WW approximation takes the following form [69, 70]:

$$\begin{aligned} & \left. \frac{d\sigma(p + P_i \rightarrow p' + P_f + k)}{d(pk)d(kP_i)} \right|_{\text{WW}} = \\ & = \frac{\alpha\chi}{\pi(p'P_i)} \left. \frac{d\sigma(p + q \rightarrow k + p')}{d(pk)} \right|_{t=t_{\min}}, \end{aligned} \quad (19)$$

where $\alpha = e^2/(4\pi) \simeq 1/137$ is the fine structure constant, and the flux of virtual photon χ from the nucleus is expressed through the elastic form-factor $F(t)$ as:

$$\chi = Z^2 \int_{t_{\min}}^{t_{\max}} \frac{t - t_{\min}}{t^2} F^2(t) dt, \quad (20)$$

where the typical upper limit is chosen to be

$$t_{\max} \simeq m_{\text{MED}}^2 + m_l^2, \quad (21)$$

according to Refs. [72, 73], and t_{\min} is defined below by Eq. (23). Using the Jacobian of the transformation from (k, p) and (k, P_i) to $\cos(\theta_{\text{MED}})$ and $x = E_{\text{MED}}/E_l$ variables in the case of an ultra-relativistic incident lepton in the laboratory frame, one can get:

$$\begin{aligned} & \left. \frac{d\sigma(p + P_i \rightarrow p' + P_f + k)}{dx d\cos(\theta_{\text{MED}})} \right|_{\text{WW}} = \frac{\alpha\chi}{\pi} \cdot \\ & \cdot \left. \frac{E_l^2 x \beta_{\text{MED}}}{1-x} \frac{d\sigma(p + q \rightarrow k + p')}{d(pk)} \right|_{t=t_{\min}}, \end{aligned} \quad (22)$$

where $\beta_{\text{MED}} = \sqrt{1 - m_{\text{MED}}^2/(xE_l)^2}$ is the typical velocity of the mediator.

Using conditions on the mass shell in the form $p' = m_l^2$ and assuming the collinearity of the vector \mathbf{q} with the vector $\mathbf{k} - \mathbf{p}$, one can obtain the minimum value of virtuality in WW approximation t_{\min}^{WW} as:

$$t_{\min}^{\text{WW}} \simeq U^2/(4E_l^2(1-x)^2), \quad (23)$$

where we denote the following function

$$U \equiv m_l^2 - u_2 \simeq E_l^2 \theta_{\text{MED}}^2 x + m_{\text{MED}}^2 (1-x)/x + m_l^2 x > 0. \quad (24)$$

The Mandelstam variables can be expressed through the both x and θ_{MED} variables:

$$u_2 = (p - k)^2 = m_l^2 - U \lesssim 0, \quad (25)$$

$$t_2 = (p - p')^2 \simeq -Ux/(1-x) + m_{\text{MED}}^2 \lesssim 0, \quad (26)$$

$$s_2 = (p' + k)^2 \simeq U/(1-x) + m_l^2 \gtrsim 0. \quad (27)$$

In Eqs. (23), (25), (26), and (27), we keep only leading terms, neglecting the sub-leading contributions

from [102]

$$\frac{m_{\text{MED}}^2}{E_{\text{MED}}^2} \ll 1, \quad \frac{m_l^2}{(E_l')^2} \ll 1, \quad \theta_{\text{MED}} \ll 1, \quad \frac{|\mathbf{q}|}{E_l'} \ll 1. \quad (28)$$

Both the energy conservation law, $q_0 + E_l = E_l' + E_{\text{MED}}$, and the condition, $q_0/E_l \ll 1$, imply that $E_l \simeq E_{\text{MED}} + E_l'$. Thus, one can get minimum and maximum values of energy fractions, $x = E_{\text{MED}}/E_l$, in the following forms $x_{\text{min}} \simeq m_{\text{MED}}/E_l$ and $x_{\text{max}} \simeq 1 - m_l/E_l$, respectively.

In the so-called improved WW (IWW) approach [73, 101] the dependence of t_{min} on x and θ_{MED} in the flux derivation is omitted to simplify calculations, which is important for the integration that exploits Monte-Carlo (MC) methods [58], such that

$$t_{\text{min}}^{\text{IWW}} \simeq m_{\text{MED}}^4/(4E_l'^2). \quad (29)$$

This means; however, that the IWW approach is less accurate [73]. We also note that the following inequalities hold for the wide range of parameter space,

$$t_{\text{min}}^{\text{WW}} \gtrsim t_{\text{min}}^{\text{IWW}}, \quad (30)$$

$$t_{\text{min}}^{\text{WW}}(x = x_{\text{max}}) \gtrsim \max\left(\frac{m_l^2}{4}, \frac{E_0^4}{4m_l^2}\theta_{\text{MED}}^4\right), \quad (31)$$

which can be helpful for the shape analysis of the differential cross section.

In the case of spin-0 and spin-1 mediators, the matrix element for the Compton-like process

$$l^\pm(p) + \gamma(q) \rightarrow l^\pm(p') + \text{MED}(k), \quad (32)$$

can be written as:

$$i\mathcal{M}_{2 \rightarrow 2}^{\text{MED}} = ic_{ll}^{\text{MED}} e\mathcal{L}^\mu \varepsilon_\mu(q), \quad (33)$$

where $\varepsilon_\nu(q)$ is polarization vector for off-shell incoming photon from nucleus. The differential cross section for process $2 \rightarrow 2$ is:

$$\frac{d\sigma(p+q \rightarrow k+p')}{d(pk)} = -\frac{(c_{ll}^{\text{MED}})^2 e^2 |\mathcal{A}_{2 \rightarrow 2}^{\text{MED}}|^2}{8\pi(s_2 - m_l^2)^2}, \quad (34)$$

where $|\mathcal{A}_{2 \rightarrow 2}^{\text{MED}}|^2$ is the amplitude squared of the Compton-like processes that are collected in (B3) - (B6).

IV. THE BREMSSTRAHLUNG-LIKE CROSS SECTIONS

In this section, we consider the cross sections in the cases of WW and ETL approximations for various benchmark parameters. The total and differential cross sections are calculated by the numerical integration in the case of the specific experimental setups. It is worth mentioning that the general behavior of the cross sections for scalar, pseudoscalar, vector and axial-vector mediators is similar; thus, we show for the specific cases only the differential cross section for the scalar or vector mediator. Also, we use Tsai-Shiff's form-factor as a benchmark one for the cross section in the WW and ETL approxi-

mations [58, 65, 102, 119]. Moreover, in the case of the WW approximation and Tsai-Shiff's form-factor we have an analytical form of the differential cross section [19], and some auxiliary integrals for that are provided in Appendix B.

For a calculation of the matrix elements and a numerical integration we use the FEYNCALC package [120, 121] and the WOLFRAM MATHEMATICA routine [122], respectively. The global adaptive strategy and the Gauss-Kronrod method for numerical integration in MATHEMATICA package are exploited.

A. The double-differential cross section

In Fig. 1 we show the double-differential cross section as a function of MED emission angle θ_{MED} for various experiments, benchmark masses, m_{MED} , and some typical energy fractions x . The double-differential cross section has a similar dependence on the mediator radiation angle θ_{MED} with fixed $x = \text{const}$ for each types of mediators, so that only the case of scalar MED in Fig. 1 is shown. Also, for the fixed x the double-differential cross section grows as a power law function of θ_{MED} to some typical angle $\theta_{\text{typ}}^{2\text{D}}$ at which it peaks and rapidly declines. Moreover, the larger benchmark value of x the smaller typical angle $\theta_{\text{typ}}^{2\text{D}}$ in the case of $m_l \lesssim m_{\text{MED}}$. In addition, the typical angle $\theta_{\text{typ}}^{2\text{D}}$ shifts slowly toward larger values of angle θ_{MED} for the increasing mass of the MED. In particular, the typical angle $\theta_{\text{typ}}^{2\text{D}}$ of the double-differential cross section lies in the range from $\mathcal{O}(10^{-6})$ to $\mathcal{O}(10^{-3})$ for $x \simeq 1$ in the MED mass range from 1 MeV to 1 GeV. Also, for intermediate values of x , the typical angle $\theta_{\text{typ}}^{2\text{D}}$ takes values from $\mathcal{O}(10^{-5})$ to $\mathcal{O}(10^{-2})$. For small $x \ll 1$ the typical angle $\theta_{\text{typ}}^{2\text{D}}$ ranges from $\mathcal{O}(10^{-4})$ to $\mathcal{O}(10^{-1})$. Note that the the region of relatively large angle $\theta_{\text{MED}} \gtrsim \theta_{\text{typ}}^{2\text{D}}$ the ETL cross section can be approximated by a power-law function of θ_{MED} ; however, the WW cross section has a sharp cut-off. In particular, sharp cutting occurs in range from $\mathcal{O}(10^{-2})$ to $\mathcal{O}(10^{-1})$ in the case of large $x \simeq 1$, and in area from $\mathcal{O}(10^{-1})$ to $\mathcal{O}(10^0)$ in the case of small values of $x \ll 1$. We discuss analytical derivation of the corresponding cut-off angle and $\theta_{\text{typ}}^{2\text{D}}$ in Appendix C.

We note that the large values of x provide the dominant contribution to the total cross section in the case of $m_l \lesssim m_{\text{MED}}$. As a result, one can use the typical cut-off angle $\theta_{\text{max}} \simeq 0.1$ for the total cross section calculations in order to reduce the integration time. The latter can be crucial for optimization of a realistic MC simulation of Dark Sector bremsstrahlung, implying sufficiently large statistics of leptons accumulated on target [123–125].

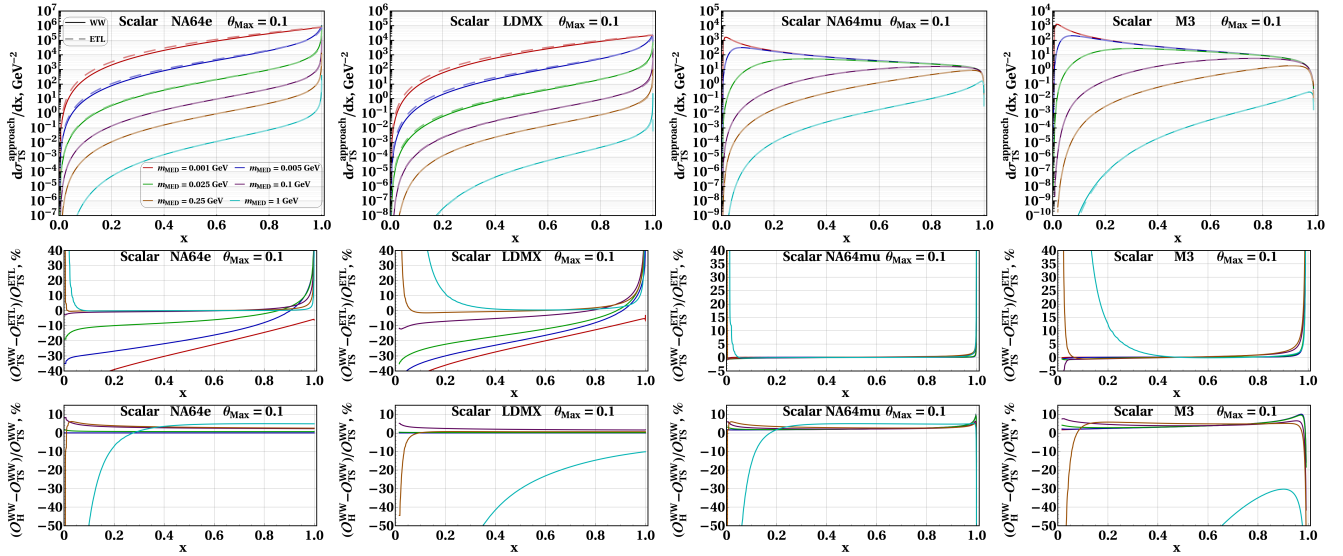


FIG. 2. The differential cross sections as a function of energy fraction x in case of scalar mediator for various experiments, such as NA64e, LDMX, NA64 μ , and M³. We also set $\theta_{\max} = 0.1$ and $c_{II}^{\text{MED}} = 1$. The curve colors correspond to fixed values of the mediator masses. In the upper row we show the differential cross sections for different masses, where the solid and dashed lines correspond to the WW and ETL approximations. In the middle rows we show the relative difference of differential cross sections between the WW and ETL approximations. In the bottom row we show the relative difference between the differential cross sections calculated for Helm's (13) and Tsai-Schiff's (12) form-factors.

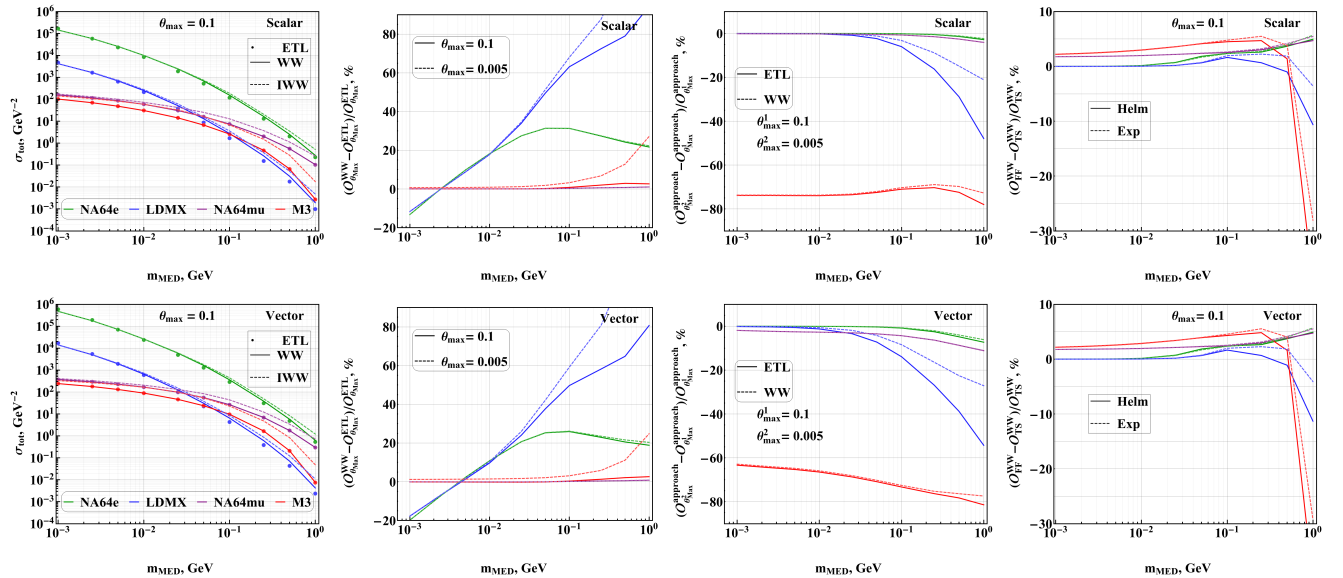


FIG. 3. The total cross section σ_{tot} as a function of its mass m_{MED} for benchmark Tsai-Schiff's form-factor. No energy fraction cuts are imposed on the cross sections. The first and second rows of figures correspond to scalar and vector mediators, respectively. Green, blue, purple and red lines correspond to NA64e, LDMX, NA64 μ and M³ experiments, respectively. In the first column the total cross sections with benchmark $\theta_{\max} = 0.1$ are shown. The solid lines, dashed lines and dots correspond to calculations for WW, IWW, and ETL approximations, respectively. In the second column the relative differences of total cross sections are shown for the WW and ETL approximations implying the different maximum angles of mediator emission. The solid and dotted lines correspond to the $\theta_{\max} = 0.005$ and $\theta_{\max} = 0.1$, respectively. In the third column the relative differences of total cross sections are shown for angles 0.005 and 0.1 for the specific approximations. The solid and dashed lines correspond to the ETL and WW approximations, respectively. In the fourth column the relative differences of total cross sections are shown in the case of the WW approximation for different form-factors. The solid and dashed lines correspond to the Helm (13) and exponential (14) form-factors, respectively.

B. The differential cross section

In Fig. 2 we show the comparison between WW and ETL differential cross sections for the specific parameter

set. A description of the typical differential cross sec-

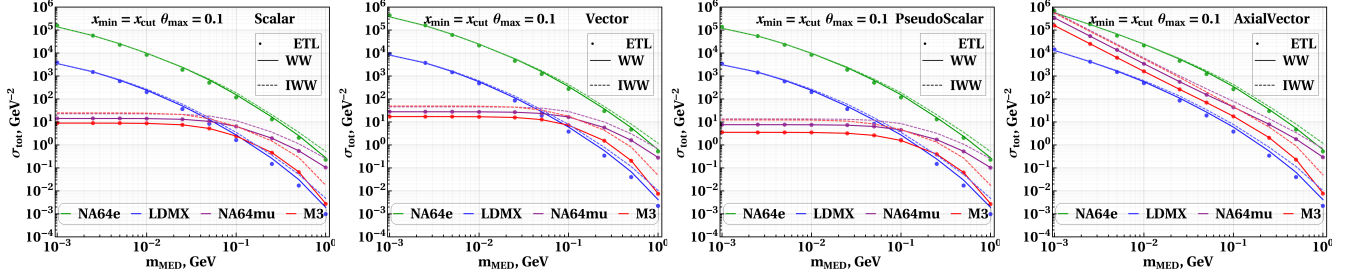


FIG. 4. The total cross sections σ_{tot} with typical angle cut $\theta_{\text{max}} = 0.1$ in the case of the missing energy signatures, where the benchmark Tsai-Schiff's form-factor is chosen. The energy fraction cuts, x_{cut} , for the cross sections are in Tab. I. The plots show the cases of scalar, vector, pseudoscalar and axial-vector mediators. The green, blue, purple and red lines correspond to NA64e, LDMX, NA64 μ , and M³ experiments, respectively. Solid line, dashed line and dots correspond to calculations for WW, IWW, and ETL approximations, respectively.

tion shapes are shown in the following. In the case of the electron mode, differential cross section has a very sharp peak in the region of the relatively large energy fraction $x \simeq 1$. Moreover, the larger m_{MED} the sharper peak. In the case of the muon mode, the peak of cross section occurs near $x \ll 1$ for small MED masses and near $x \simeq 1$ for large MED masses. In addition, the peak of cross section is mitigated in the case of a muon primary beam that can be explained as follows. For the peak forward limit $x \simeq 1$ of electron mode, one can estimate that $t_{\text{min}}^{\text{WW}} \gtrsim \mathcal{O}(m_e^2)$, thus the cross section acquires a relatively large values in the sharp peak region (see, e. g. Eq. (31) for detail). However, for the muon beam a naive inequality also holds $t_{\text{min}}^{\text{WW}} \gtrsim \mathcal{O}(m_\mu^2)$, as a result that suppresses the muon cross section for $x \simeq 1$. For the peak forward region $x \simeq 1$ the validity of the WW approach can be broken for the electron beam mode, as a result that can provide relatively large uncertainty $\mathcal{O}(80)\%$ to the total cross section calculated with respect to the ETL method, as we will see below in Sec. IV C.

Next, we consider the relative difference between the differential cross sections calculated in the WW and ETL approaches for various experiments. NA64e: for the relatively large masses $m_{\text{MED}} \gtrsim 100$ MeV, the using of WW approximation leads to overestimation at the level of $\mathcal{O}(10)\%$ around $x \simeq 1$. However, for intermediate and small masses of MED, an underestimation occurs around $\mathcal{O}(10)\%$ in case of small values $x \ll 1$ for the WW approximation. NA64 μ : overestimation occurs only near the boundaries $x \ll 1$ and $x \simeq 1$ and reaches $\mathcal{O}(10)\%$. LDMX and M³: the behavior of the relative differences is similar to the shapes of NA64e and NA64 μ , respectively, but the overestimation for the large masses starts to increase for the typical intermediate range $x \lesssim 1$.

The impact of different form-factors on the differential cross sections in the WW approximation is discussed below. The effects of screening and the different size description of the nucleus are associated with the mediator mass at the typical scales $m_{\text{MED}} \simeq (4E_0^2 t_a)^{1/4}$ and $m_{\text{MED}} \simeq (4E_0^2 t_d)^{1/4}$, respectively (see, e. g. Eq. (30) for detail). Note that the screening by atomic electrons

impacts on form-factors only for small mass of MED as t_{min} reaches the typical value t_a . In particular, the relative differences of differential cross sections with and without the screening are $\lesssim \mathcal{O}(100)\%$ and $\lesssim \mathcal{O}(10)\%$ in the cases of electron and muon modes implying a small mass of MED, respectively. Similarly, the relative differences are $\lesssim \mathcal{O}(1)\%$ and $\lesssim \mathcal{O}(0.1)\%$ in the cases of electron and muon modes for intermediate mass region $m_{\text{MED}} \gtrsim 100$ MeV. Finally, for large masses of MED, $m_{\text{MED}} \lesssim 1$ GeV, one can neglect the screening effect.

Let us exploit the results of Refs. [72, 73, 102] for IWW differential cross sections to estimate the typical energy fraction for small masses of the mediator, $m_{\text{MED}} \lesssim m_l$. The authors of Refs.[72, 73, 102] show that the θ_{MED} can be integrated out analytically in Eq. (22) for IWW case and the regarding typical differential cross section is estimated to be

$$\left(\frac{d\sigma_{2\rightarrow 3}}{dx}\right)_{\text{IWW}} \propto P_{\text{MED}}(x) \left(m_{\text{MED}}^2 \frac{1-x}{x} + m_l^2 x\right)^{-1}, \quad (35)$$

where $P_{\text{MED}}(x)$ is a polynomial function of x that is defined by the specific type of the mediator.

For sufficiently light mediators, $m_{\text{MED}} \lesssim m_l$, one can estimate the the peak position of the cross sections by using Eq. (35). The denominator of the Eq. (35) has its minimum at $x \simeq m_{\text{MED}}/m_l$. Remarkably, that $x \simeq m_{\text{MED}}/m_l$ is quite good approximation for the peak position of the IWW cross section for sufficiently light mediators, $m_{\text{MED}} \lesssim m_l$. However, near $m_{\text{MED}} \simeq m_l$ the term $P_{\text{MED}}(x)$ can impact on the cross section peak position, such that $x \simeq m_{\text{MED}}/m_l$ does not describe the position of the maximum accurately. The latter analytical calculations are rather tedious and beyond the scope of the present paper.

Now let us discuss typical energy fraction for sufficiently heavy mediators, $m_{\text{MED}} \gtrsim m_l$. The kinematical constraint on x implies that $E_l \simeq E_{\text{MED}} + m_l$ for the initial lepton transferring its entire momentum to the mediator. It means that the typical energy fraction $x \lesssim x_{\text{typ}} \simeq 1 - m_l/E_l$ for heavy mediators, $m_{\text{MED}} \gtrsim m_l$, at which the IWW cross section peaks.

As results, the typical peak position of the differential cross section is estimated to be

$$x_{\text{typ}} \simeq \min\left(1 - \frac{m_l}{E_l}, \frac{m_{\text{MED}}}{m_l}\right), \quad (36)$$

which holds either for $m_{\text{MED}} \lesssim m_l$ or $m_{\text{MED}} \gtrsim m_l$. Moreover, Eq. (36) also holds for both the ETL and WW cross sections, since their maxima almost coincide with the peak position of the IWW cross section [72, 73].

We also note that the inequalities $m_{\text{MED}}/E_{\text{MED}} \ll 1$ and $m_l/E_l' \ll 1$ can be violated at the boundary points $x \ll 1$ and $x \simeq 1$, respectively. As a result, this can lead to the discrepancy between the ETL and WW differential cross-section $d\sigma_{2 \rightarrow 3}/dx$, that is depicted in Fig. 2, i. e. the typical magnitude of $(O_{\text{WW}} - O_{\text{ETL}})/O_{\text{ETL}}$ can be as large as 50% for $x \ll 1$ and $x \simeq 1$.

C. The total cross section

In Fig. 3 we show the total cross sections as a functions of m_{MED} in the case of various experiments for vector and scalar MEDs without cuts. In Fig. 4 we show the total cross sections as a functions of m_{MED} implying the cuts x_{cut} collected in Table. I for all types of the mediator. The obtained curves of the total cross section with the cuts x_{cut} in this section can be used to calculate the constraints on the corresponding coupling constant [126] implying the missing energy signatures, $l^\pm N \rightarrow l^\pm N + \text{MED}(\rightarrow \chi\bar{\chi})$. The latter, however, is beyond the scope of the present paper.

Let us discuss first the impact of maximum angle of MED emission θ_{max} on the validation of WW approach. The value of angle θ_{max} can be set by implying the geometry of the experimental detectors [72, 73] and the optimization of MC simulation of the MED emission (numerical calculations of the total and differential cross sections, say in DMG4 package [123, 124], so that the setting of optimal angle can significantly reduce the computing time of the simulation). Moreover, an optimal value of the angle θ_{max} can be considered as a parameter of interest, which impacts the validity of WW approach.

However, the accuracy of calculations in the WW approximation with different values of angle θ_{max} is sensitive to the choice of the experimental parameters shown in Tab. I. In particular, the angle $\theta_{\text{max}} \simeq 0.005$ was used for the analysis of the WW approximation [72, 73] due to the geometrical setup of the experiment E137 with relatively long base-line of $\mathcal{O}(100)$ m. The latter is linked to the acceptance of the fixed target facility implying the visible decay of $\text{MED} \rightarrow e^+e^-$ in the fiducial volume and its production process $e^-N \rightarrow e^-N + \text{MED}$. Therefore, the corresponding angle $\theta_{\text{max}} = 0.005$ is considered as a benchmark one in the present article.

This is not the case for the production of the MED in the bremsstrahlung-like reaction $\mu N \rightarrow \mu N + \text{MED}$ followed by its invisible decay into DM particles $\text{MED} \rightarrow \chi\bar{\chi}$ for NA64e and NA64 μ facilities. The acceptance angle

constraints $\theta \ll 1$ can be mitigated for the experiments with short base-line of $\mathcal{O}(1)$ m, such that the relatively large emission angles can be important $\theta_{\text{max}} \lesssim 0.1$ for proper calculation of the total cross section. In addition, the optimal value of the angle θ_{max} leads to reducing the computing time of the numerical calculations, where the contribution to the cross section in the range $\theta \gtrsim \theta_{\text{max}}$ is discarded as negligible. In particular, the corresponding analysis was performed for the experiment NA64 μ [19, 57–59] using the simulation package DMG4 [123, 124], where the optimal value of angle was chosen to be $\theta_{\text{max}} = 0.1$. Thus, the typical value $\theta_{\text{max}} = 0.1$ is exploited as a second benchmark angle in the present paper. It is also worth noting that the ETL total cross section in the case of angles $\theta_{\text{max}} = 0.1$ and $\theta_{\text{max}} = \pi$ has a relative difference at the level of $\lesssim \mathcal{O}(0.1)$ % for all experiments of interest and all mediators.

The relatively large difference between WW and ETL total cross sections for the angles $\theta_{\text{max}} = 0.1$ and $\theta_{\text{max}} = 0.005$ arises only for the LDMX and M^3 experiments for $\mathcal{O}(100)$ MeV $\lesssim m_{\text{MED}} \lesssim \mathcal{O}(1)$ GeV mass range. Indeed, the typical mediator radiation angle lies in the range of large angle for these experiments that refers to a small primary beam energy relative to the corresponding mediator mass. Also, the typical angle of MED emission can be estimated as follows $\theta \simeq m_l/E_l$. Moreover, in the case of the M^3 experiment, typical angles are $\simeq \mathcal{O}(10^{-2})$, which lead to a significant cross section underestimation for $\theta_{\text{max}} = 0.005$ if one compares it with $\theta_{\text{max}} = 0.1$.

Now let us discuss the difference between the WW and ETL approximations for the typical benchmark angle $\theta_{\text{max}} = 0.1$. In the region of large masses, the relative difference is at the level of $\mathcal{O}(20)$ % for the NA64e experiment. However, for the LDMX experiment, the relative difference grows significantly to the level of $\mathcal{O}(100)$ % as mediator mass increases. In the case of the NA64 μ and M^3 experiments, the relative difference is sufficiently small $\lesssim \mathcal{O}(1)$ % for the entire range of mediator masses and it grows with increasing mass. The dominant overestimation of the WW cross section is associated with a peak forward region, $x \simeq 1$, for large masses $m_{\text{MED}} \gtrsim 100$ MeV. However, in the case of small masses $m_{\text{MED}} \lesssim 100$ MeV, an underestimation in the WW method occurs in the region $x \lesssim 1$.

The relative difference of the total cross sections for different atomic form-factors is discussed below. For the mediator of different types and masses $m_{\text{MED}} \lesssim 100$ MeV the difference in total cross-section is $\lesssim \mathcal{O}(5)$ % in the case of electron and muon mode. Also, for the NA64 experiments with high-energy leptons with $E_{e/\mu} \gtrsim 100$ GeV, the relative difference in total cross section for large mediator masses can be as small as $\lesssim \mathcal{O}(5)$ %. However, the relative difference for LDMX and M^3 experiments reaches $\mathcal{O}(10)$ % for $m_{\text{MED}} \lesssim 1$ GeV.

To conclude this section, let us discuss the origin of the

discrepancy between ETL and WW (IWW) cross sections for the electron beam mode. We adopt the results of Refs. [72, 73] that provided a link between full $2 \rightarrow 3$ and $2 \rightarrow 2$ matrix elements:

$$\frac{1}{8M^2} \int \frac{d\phi}{2\pi} |\mathcal{A}_{2 \rightarrow 3}^{\text{MED}}|^2 \simeq \frac{t - t_{\min}}{2t_{\min}} |\mathcal{A}_{2 \rightarrow 2}^{\text{MED}}|^2 \Big|_{t=t_{\min}}. \quad (37)$$

This approximate expression relies on the conditions (28) and implies that the virtual photon momenta \mathbf{q} and $\mathbf{k} - \mathbf{p}$ are highly collinear. The explicit expressions of $|\mathcal{A}_{2 \rightarrow 3}^{\text{MED}}|^2$ and $|\mathcal{A}_{2 \rightarrow 2}^{\text{MED}}|^2$ are given by (A14) - (A17) and (B3) - (B6), respectively. Moreover, Eq. (37) implies that all virtual photons with $t \gtrsim t_{\min}$ can contribute to the mediator production.

On the other hand, in case of electron beam mode (i. e. for LDMX and NA64e experiments) a main contribution to the single-differential cross section is associated with the peak forward singularity region at $x \simeq 1$ for large masses $m_{\text{MED}} \lesssim 1$ GeV of mediator. The conditions (28) can be violated, $|\mathbf{q}| \lesssim E_e(1-x)$, for sufficiently large energy fraction values $x \simeq 1$ and relatively small energy of LDMX, $E_e \simeq 16$ GeV. In addition, the above-mentioned momenta collinearity between \mathbf{q} and $\mathbf{k} - \mathbf{p}$ can be also violated in the peak forward singularity region (see e. g. Refs. [69, 70, 102] for detail).

As a result, there is an overestimation in both IWW and WW cross sections if one compares these with ETL one. Say, for the LDMX experiment the regarding discrepancy can be as large as 80%. However, for the NA64e facility with larger beam energy, $E_e \simeq 100$ GeV, compared to LDMX, the error is estimated to be at the level of 20% for heavy mediator, $m_{\text{MED}} \lesssim 1$ GeV.

V. CONCLUSION

In the present paper we have discussed in detail the calculation of the MED production cross sections in the case of ETL and WW approaches for fixed-target experiments, such as NA64e, LDMX, NA64 μ and M³. Scalar, pseudoscalar, vector, and axial-vector types of particle are chosen as hidden sector MEDs, that are produced in the bremsstrahlung-like reaction $l^\pm N \rightarrow l^\pm N + \text{MED}$. Our study shows that the mass (electron or muon) of the incident beam particles and their energy ($E_{e/\mu} \simeq 15$ GeV for LDMX and M³ or $E_{e/\mu} \gtrsim 100$ GeV for NA64e and NA64 μ) in the fixed-target experiments can impact the validity of the WW approach for the calculation of the bremsstrahlung-like total cross section. The relative difference of total cross sections varies from $\mathcal{O}(1)$ % to $\mathcal{O}(10)$ % for a muon mode and from $\mathcal{O}(-20)$ % to $\mathcal{O}(80)$ % for an electron mode. The main difference between two approaches for electron beam mode arises from peak forward singularity of the cross section. In addition, we show that the exploiting of the various atomic form-factor parameterization leads to the cross section relative difference at the level of $\lesssim \mathcal{O}(10)$ %.

ACKNOWLEDGMENTS

We would like to thank A. Celentano, P. Crivelli, S. Demidov, R. Dusaev, S. Gninenko, D. Gorbunov, M. Kirsanov, N. Krasnikov, E. Kriukova, V. Lyubovitskij, L. Molina Bueno, A. Pukhov, A. Shevelev, H. Sieber, and A. Zhevlakov for very helpful discussions and correspondences. This work was supported by the Foundation for the Advancement of Theoretical Physics and Mathematics BASIS (Project No. 24-1-2-11-2 and No. 24-1-2-11-1). This research was supported by the Ministry of Education and Science of the Russian Federation in part of the Science program (Project FSWW-2023-0003).

VI. DATA AVAILABILITY

The data that support the findings of this article are openly available [127].

Appendix A: Cross section of bremsstrahlung-like process

In this section we calculate the cross section in case of the mediator production by a lepton scattering off the heavy nucleus for the exact tree-level approach. In particular, the differential cross section of the process (5) takes the form:

$$d\sigma_{2 \rightarrow 3} = \frac{|\overline{\mathcal{M}}_{2 \rightarrow 3}^{\text{MED}}|^2}{4I} d\Pi, \quad (A1)$$

and the Lorentz invariant volume of momentum space is:

$$d\Pi = \frac{(2\pi)^4 \delta^{(4)}(p + q - p' - k) d\mathbf{p}' d\mathbf{P}_f d\mathbf{k}}{(2\pi)^3 2E_{p'} (2\pi)^3 2E_{P_f} (2\pi)^3 2E_k}, \quad (A2)$$

where $I = \sqrt{(p, P_i)^2 - m_i^2 M^2} = |\mathbf{p}|M$ is Miller's invariant, which characterizes the flow of initial particles. For integration over the final states of the process $2 \rightarrow 3$, one can choose four independent variables as: the azimuthal ϕ_q angle of the vector $\mathbf{q} = -\mathbf{P}_f$, the virtuality of photon t , angle $\theta_{\text{MED}} = \angle(\mathbf{k}, \mathbf{p})$ and the energy ratio of the mediator and initial particle $x = k_0/p_0$ [72].

Next, to obtain a double differential cross section based on the mediator parameters, we use the following frame. The Oz axis is parallel to the spatial part of the vector $\mathbf{V} \equiv \mathbf{k} - \mathbf{p}$ and the vector \mathbf{k} lies in the xOz plane. One can get the following formulas:

$$\cos(\theta_q) = (|\mathbf{q}|^2 + |\mathbf{V}|^2 - |\mathbf{p}'|^2) / (2|\mathbf{q}||\mathbf{V}|), \quad (A3)$$

$$|\mathbf{V}|^2 = |\mathbf{p}|^2 + |\mathbf{k}|^2 - 2|\mathbf{p}||\mathbf{k}| \cos(\theta_{\text{MED}}), \quad (A4)$$

where we exploit $|\mathbf{p}'|^2 = (q_0 - V_0)^2 - m_i^2$ and $V_0 = -E_l(1-x) < 0$. However, by taking into account inequalities $q_0 < 0$ and $E_l' > m_l$, a kinematic constraint on the photon virtually yields

$$t \leq 2M(E_l(1-x) - m_l). \quad (A5)$$

By taking into account the expression $(q - V)^2 = p'^2$, the spatial transferred momentum \mathbf{q} is expressed through the polar angle θ_q as:

$$|\mathbf{q}| = \frac{|\mathbf{V}| \cos(\theta_q)(\tilde{u} + 2Md_{V_0}) + d_{V_0}\sqrt{D}}{2d_{V_0}^2 - 2|\mathbf{V}|^2 \cos^2(\theta_q)}, \quad (\text{A6})$$

where we introduce the notations:

$$D = 4M^2|\mathbf{V}|^2 \cos^2(\theta_q) + \tilde{u}^2 + 4Md_{V_0}\tilde{u},$$

$$d_{V_0} = (M - V_0) = E'_l + P_{f_0} > 0.$$

Further, the Mandelstam-like variables \tilde{s} and \tilde{u} can be expressed through the selected independent variables in the following form:

$$\tilde{u} = m_{\text{MED}}^2 - 2(p, k) \quad \tilde{s} = -t + 2(p, q), \quad (\text{A7})$$

where corresponding dot products are:

$$(p, k) = E_0^2 x - |\mathbf{p}||\mathbf{k}| \cos(\theta_{\text{MED}}),$$

$$(p, q) = q_0 E_l - (\mathbf{p}_x \mathbf{q}_x + \mathbf{p}_z \mathbf{q}_z).$$

Also, by taking into account that vector \mathbf{p} lies in the plane xOz , the projections of momenta \mathbf{p} and \mathbf{q} take the form:

$$\mathbf{p}_x = |\mathbf{p}| \sin(\theta_{p_z}), \quad \mathbf{p}_z = |\mathbf{p}| \cos(\theta_{p_z}),$$

$$\mathbf{q}_x = |\mathbf{q}| \sin(\theta_q) \cos(\phi_q), \quad \mathbf{q}_z = |\mathbf{q}| \cos(\theta_q),$$

and the cosine of the angle between momenta \mathbf{p} and \mathbf{V} is:

$$\cos(\theta_{p_z}) = -(|\mathbf{p}|^2 + |\mathbf{V}|^2 - |\mathbf{k}|^2) / (2|\mathbf{p}||\mathbf{V}|).$$

Next, we obtain an expression for the double differential cross section in terms of the mediator parameters. Using the delta functions $\delta^{(3)}(\mathbf{p} + \mathbf{q} - \mathbf{p}' - \mathbf{k})$ and $\delta(E_p + q_0 - E_{p'} - E_k)$, integration is performed over \mathbf{p}' and $\cos(\theta_q)$ where it is taking into account the expression [84]:

$$\begin{aligned} \delta(E_p + q_0 - E_{p'} - E_k) &= \\ &= \frac{E'_l}{|\mathbf{q}||\mathbf{V}|} \frac{\delta(f(|\mathbf{q}|) - \cos(\theta_q))}{\sqrt{M^2 + |\mathbf{q}|^2}} \Theta(1 - \cos^2(\theta_q)), \end{aligned} \quad (\text{A8})$$

where $f(|\mathbf{q}|)$ is the right hand side of the expression (A3) and the Heaviside function $\Theta(x)$ arises due to the finite limits. For the invariant volume the following expression reads:

$$d\Pi \rightarrow \frac{M}{32\pi^4} \Theta(1 - \cos^2(\theta_q)) \frac{dt}{8M^2} \frac{d\phi_q}{2\pi} \frac{d\mathbf{k}}{|\mathbf{V}|E_l x} \rightarrow \frac{2\pi M}{32\pi^4} \Theta(1 - \cos^2(\theta_q)) \frac{|\mathbf{k}|E_l}{|\mathbf{V}|} \frac{dt}{8M^2} \frac{d\phi_q}{2\pi} d\cos(\theta_{\text{MED}}) dx \frac{d\phi_k}{2\pi}, \quad (\text{A9})$$

where it is taken into account that

$$dt = M(M^2 + |\mathbf{q}|^2)^{-1/2} d|\mathbf{q}|^2.$$

As a result, the double differential cross section for the process of mediator radiation on the nucleus in terms of x and $\cos(\theta_{\text{MED}})$ takes the form: [72]:

$$\begin{aligned} \frac{d\sigma_{2 \rightarrow 3}}{dx d\cos(\theta_{\text{MED}})} &= \frac{1}{64\pi^3} \frac{|\mathbf{k}|E_l}{|\mathbf{p}||\mathbf{k} - \mathbf{p}|} \\ &\cdot \int_{t_{\min}}^{t_{\max}} dt \frac{1}{8M^2} \int_0^{2\pi} \frac{d\phi_q}{2\pi} |\mathcal{M}_{2 \rightarrow 3}^{\text{MED}}|^2. \end{aligned} \quad (\text{A10})$$

The limits of integration over the photon virtuality are expressed from the condition $|\cos(\theta_q)| < 1$ and takes the values $t_{\max} = t(Q_+)$ and $t_{\min} = t(Q_-)$ with the introduced notation:

$$Q_{\pm} = \left| \frac{|\mathbf{V}| [\tilde{u} + 2Md_{V_0}] \pm d_{V_0}\sqrt{D_0}}{2d_{V_0}^2 - 2|\mathbf{V}|^2} \right|, \quad (\text{A11})$$

where $D_0 = 4M^2|\mathbf{V}|^2 + \tilde{u}^2 + 4Md_{V_0}\tilde{u}$. Note that

the condition $D_0 > 0$ yields an additional kinematic constraint.

It is also worth noting that the given set of variables allows us to obtain a differential cross section in terms of outgoing lepton parameters. In particular, one can use the replacement:

$$k \leftrightarrow p', \quad x \rightarrow y = p'_0/p_0, \quad \theta_{\text{MED}} \rightarrow \psi_{\nu}. \quad (\text{A12})$$

where ψ_{ν} is angle between the direction of the momenta \mathbf{p} and \mathbf{p}' .

The the matrix element squared for the process $2 \rightarrow 3$ can be written as:

$$|\overline{\mathcal{M}}_{2 \rightarrow 3}^{\text{MED}}|^2 = C_{\mathcal{M}}^2 |\mathcal{A}_{2 \rightarrow 3}^{\text{MED}}|^2, \quad (\text{A13})$$

where we define $C_{\mathcal{M}} = c_{\text{il}}^{\text{MED}} e^2 Z^2 F_s(-q^2)/q^2$. For the process of radiation of scalar, pseudoscalar, vector and axialvector mediators on the nucleus, the squared amplitudes take the form, respectively [19, 58, 72, 73]:

$$\left| \mathcal{A}_{l-N \rightarrow l-N\phi}^{\phi} \right|^2 = \frac{(\tilde{u} + \tilde{s})^2}{\tilde{u}\tilde{s}} P^2 - \frac{4t(k, P)^2}{\tilde{u}\tilde{s}} - (m_{\text{MED}}^2 - 4m_l^2) \frac{(\tilde{u} + \tilde{s})^2}{\tilde{u}^2 \tilde{s}^2} \left(-P^2 t + 4 \left(\frac{\tilde{u}(p, P) + \tilde{s}(p', P)}{\tilde{u} + \tilde{s}} \right)^2 \right), \quad (\text{A14})$$

$$|\mathcal{A}_{l-N \rightarrow l-NP}^P|^2 = \frac{(\tilde{u} + \tilde{s})^2}{\tilde{u}\tilde{s}} P^2 - \frac{4t(k, P)^2}{\tilde{u}\tilde{s}} - m_{\text{MED}}^2 \frac{(\tilde{u} + \tilde{s})^2}{\tilde{u}^2 \tilde{s}^2} \left(-P^2 t + 4 \left(\frac{\tilde{u}(p, P) + \tilde{s}(p', P)}{\tilde{u} + \tilde{s}} \right)^2 \right), \quad (\text{A15})$$

$$|\mathcal{A}_{l-N \rightarrow l-NV}^V|^2 = 2 \frac{\tilde{u}^2 + \tilde{s}^2}{\tilde{u}\tilde{s}} P^2 - \frac{8t}{\tilde{u}\tilde{s}} \left((p, P)^2 + (p', P)^2 + \frac{2m_{\text{MED}}^2 - \tilde{s} - \tilde{u} - t}{2} P^2 \right) - 2(m_{\text{MED}}^2 + 2m_l^2) \frac{(\tilde{u} + \tilde{s})^2}{\tilde{u}^2 \tilde{s}^2} \left(-P^2 t + 4 \left(\frac{\tilde{u}(p, P) + \tilde{s}(p', P)}{\tilde{u} + \tilde{s}} \right)^2 \right), \quad (\text{A16})$$

$$|\mathcal{A}_{l-N \rightarrow l-NA}^A|^2 = 2 \frac{\tilde{u}^2 + \tilde{s}^2}{\tilde{u}\tilde{s}} P^2 - \frac{8t}{\tilde{u}\tilde{s}} \left((p, P)^2 + (p', P)^2 - \frac{\tilde{s} + \tilde{u} + t}{2} P^2 \right) + 4m_l^2 \frac{(\tilde{u} + \tilde{s})^2 P^2}{m_{\text{MED}}^2 \tilde{s}\tilde{u}} - \frac{16m_l^2 t(k, P)^2}{m_{\text{MED}}^2 \tilde{s}\tilde{u}} - 2(m_{\text{MED}}^2 - 4m_l^2) \frac{(\tilde{u} - \tilde{s})^2}{\tilde{u}^2 \tilde{s}^2} \left(-P^2 t + 4 \left(\frac{\tilde{u}(p, P) + \tilde{s}(p', P)}{\tilde{u} - \tilde{s}} \right)^2 \right), \quad (\text{A17})$$

where dot products are expressed as:

$$(P, P) = 4M^2 + t, \quad (k, P) = (p, P) - (p', P), \quad (p, P) = 2ME_p - (\tilde{s} + t)/2, \quad (p', P) = 2M(E_p - E_k) + (\tilde{u} - t)/2. \quad (\text{A18})$$

Appendix B: Analytical expressions for the WW approximation

The auxiliary integrals in this section can be used for analytical integration over an radiated particle angle for the differential cross section in the Weizsäcker-Williams approximation in the case of Tsai-Schiff's elastic form-factor.

In general, the differential cross section for the compton-like production of considering mediators depends on the angle via the Mandelstam variables as:

$$\frac{|\mathcal{M}_{2 \rightarrow 2}^{\text{MED}}|^2}{8\pi(s_2 - m_l^2)^2} = \frac{P(s_2, t_2, u_2)}{(s_2 - m_l^2)^3 (u_2 - m_l^2)}, \quad (\text{B1})$$

where $P(s_2, t_2, u_2)$ - polynomial function in all arguments e.g. (B3) - (B6). Also, the analytically integrated virtual photon flux with Tsai-Schiff's form-factor reads as follows [58]:

$$\chi_{TS} = \frac{Z^2 t_d^2}{(t_a - t_d)^3} \left([C_1^X + C_2^X t_{\min}] + [C_3^X + C_4^X t_{\min}] \ln \left[\frac{t_{\min} + t_d}{t_{\min} + t_a} \right] \right) \quad (\text{B2})$$

where the functions C_1^X , C_2^X , C_3^X and C_4^X are defined by the following expressions respectively:

$$C_1^X = \left(\frac{t_d(t_a - t_d)}{t_d + t_{\max}} + \frac{t_a(t_a - t_d)}{t_a + t_{\max}} - 2(t_a - t_d) + (t_a + t_d) \ln \left[\frac{(t_d + t_{\max})}{(t_a + t_{\max})} \right] \right),$$

$$C_2^X = \left(\frac{t_a - t_d}{t_d + t_{\max}} + \frac{t_a - t_d}{t_a + t_{\max}} + 2 \ln \left[\frac{t_d + t_{\max}}{t_a + t_{\max}} \right] \right),$$

$$C_3^X = -(t_a + t_d), \quad C_4^X = -2.$$

Taking into account the photon flux with Tsai-Schiff's form-factor (B2) and using expressions (25) - (27), one can show that the double differential cross section in-

cludes the typical terms U^l and $U^l \log(U^2 + a(x))$. In particular, one can replace the angular dependence θ_{MED} by a U -like variable (see Eq. (24)) and represent the analytical integration of the double differential cross section over U for the auxiliary integrals $I_1(x, U, l) = U^l$ and $I_2(x, U, l)$. The integral $I_2(x, U, l)$ takes the following form:

$$I_2(x, U, l) = \int U^l \ln \left[\frac{U^2 + b(x)}{U^2 + a(x)} \right] dU, \quad l \in \mathbb{Z},$$

that allows us to integrate over the angle the differential cross section in the case of scalar, pseudoscalar, vector and axialvector mediators. For $l = -1$ and $l = -2$ the integral $I_2(x, U, l)$ reads, respectively:

$$\int \frac{1}{x} \ln \left(\frac{x^2 + b}{x^2 + a} \right) dx = \frac{1}{2} \ln \left(\frac{b}{a} \right) \ln(x^2) - \frac{1}{2} [\text{Li}_2(-x^2/b) - \text{Li}_2(-x^2/a)]$$

$$\int \frac{1}{x^2} \ln \left(\frac{x^2 + b}{x^2 + a} \right) dx = -\frac{1}{x} \ln \left(\frac{x^2 + b}{x^2 + a} \right) + 2 \left(\frac{\arctan(x/\sqrt{b})}{\sqrt{b}} - \frac{\arctan(x/\sqrt{a})}{\sqrt{a}} \right)$$

For $0 \leq l$ the integral $I_2(x, U, l)$ reads:

$$\int x^n \ln \left(\frac{x^2 + b}{x^2 + a} \right) dx = \frac{x^{n+1}}{n+1} \ln \left(\frac{x^2 + b}{x^2 + a} \right) - \frac{2}{n+1} \sum_{m=0}^{\frac{n-(n \bmod 2)}{2}} (-1)^m \frac{x^{n+1-2m}}{n+1-2m} (b^m - a^m) + (-1)^{\frac{n-(n \bmod 2)}{2}} \frac{2}{n+1} R_{21}(x, n, a, b),$$

where auxiliary expression $R_{21}(x, n, a, b)$ takes the form:

$$R_{21}(x, n, a, b) = \begin{cases} f_{\ln}(b) - f_{\ln}(a), & n \bmod 2 = 1, \\ f_{\text{atg}}(b) - f_{\text{atg}}(a), & n \bmod 2 = 0. \end{cases}$$

with introduced definitions $f_{\ln}(b) = (1/2)b^{\frac{n+1}{2}} \ln(x^2 + b)$ and $f_{\text{atg}}(b) = b^{\frac{n+1}{2}} \arctg(x/\sqrt{b})$. For values $l < -2$ the integral $I_2(x, U, l)$ takes the following form:

$$\begin{aligned} \int x^n \ln\left(\frac{x^2 + b}{x^2 + a}\right) dx &= \\ &= \frac{x^{n+1}}{(n+1)} \ln\left(\frac{x^2 + b}{x^2 + a}\right) + R_{22}(x, -n, a, b) \end{aligned}$$

where the auxiliary expression $R_{22}(x, n, a, b)$ for odd values of n reads as follows:

$$\begin{aligned} R_{22}(x, n, a, b) &= \frac{(-1)^{\frac{n-1}{2}}}{n-1} \left\{ \left(\frac{1}{b}\right)^{\frac{n-1}{2}} \ln\left(\frac{x^2 + b}{x^2}\right) - \left(\frac{1}{a}\right)^{\frac{n-1}{2}} \ln\left(\frac{x^2 + a}{x^2}\right) \right\} + \\ &+ \frac{2}{n-1} \sum_{k=0}^{\frac{n-5}{2}} \frac{(-1)^k}{3+2k-n} \left(\left(\frac{1}{b}\right)^{k+1} - \left(\frac{1}{a}\right)^{k+1} \right) \frac{1}{x^{n-3-2k}} \end{aligned}$$

and for even values of n is:

$$\begin{aligned} R_{22}(x, n, a, b) &= (-1)^{\frac{n-2}{2}} \frac{2}{n-1} \left\{ \left(\frac{1}{b}\right)^{\frac{n-1}{2}} \arctan\left(\frac{x}{\sqrt{b}}\right) - \left(\frac{1}{a}\right)^{\frac{n-1}{2}} \arctan\left(\frac{x}{\sqrt{a}}\right) \right\} + \\ &+ \frac{2}{n-1} \sum_{k=0}^{\frac{n-4}{2}} \frac{(-1)^k}{3+2k-n} \left(\left(\frac{1}{b}\right)^{k+1} - \left(\frac{1}{a}\right)^{k+1} \right) \frac{1}{x^{n-3-2k}} \end{aligned}$$

The squared amplitudes of the compton-like processes in the cases of scalar, pseudoscalar, vector and axial-vector mediators, respectively [19, 58, 72, 73]:

$$\left| \mathcal{A}_{l^- \gamma \rightarrow l^- \phi}^\phi \right|^2 = -\frac{(\tilde{s}_2 + \tilde{u}_2)^2}{\tilde{s}_2 \tilde{u}_2} + 2 \frac{(m_{\text{MED}}^2 - 4m_l^2)}{\tilde{s}_2 \tilde{u}_2} \left(\frac{(\tilde{s}_2 + \tilde{u}_2)^2}{\tilde{s}_2 \tilde{u}_2} m_l^2 - \tilde{t}_2 - m_{\text{MED}}^2 \right), \quad (\text{B3})$$

$$\left| \mathcal{A}_{l^- \gamma \rightarrow l^- P}^P \right|^2 = -\frac{(\tilde{s}_2 + \tilde{u}_2)^2}{\tilde{s}_2 \tilde{u}_2} + 2 \frac{m_{\text{MED}}^2}{\tilde{s}_2 \tilde{u}_2} \left(\frac{(\tilde{s}_2 + \tilde{u}_2)^2}{\tilde{s}_2 \tilde{u}_2} m_l^2 - \tilde{t}_2 - m_{\text{MED}}^2 \right), \quad (\text{B4})$$

$$\left| \mathcal{A}_{l^- \gamma \rightarrow l^- V}^V \right|^2 = 4 - 2 \frac{(\tilde{s}_2 + \tilde{u}_2)^2}{\tilde{s}_2 \tilde{u}_2} + 4 \frac{(m_{\text{MED}}^2 + 2m_l^2)}{\tilde{s}_2 \tilde{u}_2} \left(\frac{(\tilde{s}_2 + \tilde{u}_2)^2}{\tilde{s}_2 \tilde{u}_2} m_l^2 - \tilde{t}_2 - m_{\text{MED}}^2 \right), \quad (\text{B5})$$

$$\left| \mathcal{A}_{l^- \gamma \rightarrow l^- A}^A \right|^2 = 4 - \left(2 + \frac{4m_l^2}{m_{\text{MED}}^2} \right) \frac{(\tilde{s}_2 + \tilde{u}_2)^2}{\tilde{s}_2 \tilde{u}_2} + 4 \frac{(m_{\text{MED}}^2 - 4m_l^2)}{\tilde{s}_2 \tilde{u}_2} \left(\frac{(\tilde{s}_2 + \tilde{u}_2)^2}{\tilde{s}_2 \tilde{u}_2} m_l^2 - \tilde{t}_2 - m_{\text{MED}}^2 \right). \quad (\text{B6})$$

where we define:

$$\tilde{s}_2 = s_2 - m_l^2, \quad \tilde{u}_2 = u_2 - m_l^2, \quad \tilde{t}_2 = t_2 - m_{\text{MED}}^2.$$

Appendix C: Typical mediator radiation angle for the double differential cross section.

In Fig. 1 we show that the WW differential cross-section falls off much more steeply with θ_{MED} than the ETL one. That can be explained by the reduced phase space of the WW cross section compared to the ETL one. In Fig. 5 we show the typical t_{max} and t_{min} as a functions of θ_{MED} for the approaches of the interest (ETL, WW,

and IWW). The intersection points of $t_{\text{max}}^{\text{WW}}$ and $t_{\text{min}}^{\text{WW}}$ functions imply $t_{\text{max}}^{\text{WW}} = t_{\text{min}}^{\text{WW}}$; therefore these points lead to the shrinking of the WW phase space to zero (the double differential cross section falls rapidly to zero at the point $\theta_{\text{cut}}^{2\text{D}}$). In particular, the cut-off angle is estimated

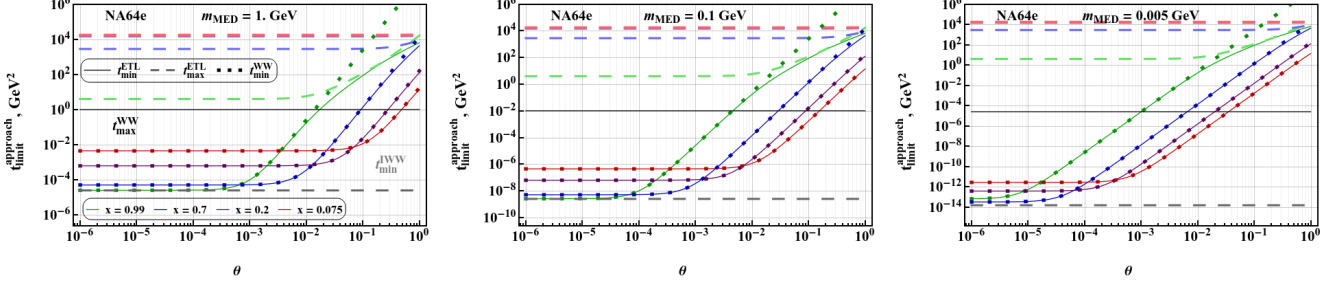


FIG. 5. The typical dependence of the maximum, t_{\max} , and minimum, t_{\min} , momentum squared on the mediator emission angle θ_{MED} for various approaches (ETL, WW and IWW) and the set of benchmark energy fraction values x . Solid (dashed) green, blue, violet and red lines show t_{\min}^{ETL} (t_{\max}^{ETL}) for $x = 0.99$, $x = 0.7$, $x = 0.2$, and $x = 0.075$, respectively. The same color dotted lines depict t_{\min}^{WW} for given benchmark set of x . The typical magnitude of t_{\max}^{WW} is estimated to be $t_{\max}^{\text{WW}} \simeq m_{\text{MED}}^2 + m_l^2$ according to Refs. [72, 73]. The latter doesn't depend on both x and θ and shown by the solid black line. We note that it implies $t_{\max}^{\text{WW}} \equiv t_{\max}^{\text{IWW}}$. Finally, the constant value of t_{\min}^{IWW} is defined by Eq. (29) and shown by gray dashed line.

to be

$$\theta_{\text{cut}}^{2\text{D}} \simeq \frac{1}{\sqrt{E_l^2 x}} \left(2E_l \sqrt{m_{\text{MED}}^2 + m_l^2} (1-x) - m_{\text{MED}}^2 \frac{(1-x)}{x} - m_l^2 x \right)^{1/2}, \quad (\text{C1})$$

from $t_{\max}^{\text{WW}} = t_{\min}^{\text{WW}}$ equation. For instance, in Fig. 5 for $x = 0.99$ and $m_{\text{MED}} = 1$ GeV we show that $t_{\max}^{\text{WW}} = t_{\min}^{\text{WW}}$ at $\theta_{\text{MED}} \simeq 10^{-2}$ for NA64e experiment. Thus, the corresponding WW differential cross section cuts at $\theta_{\text{MED}} \simeq 10^{-2}$, that is shown in Fig. 1 by solid green line in the bottom row for $m_{\text{MED}} = 1$ GeV.

On the other hand, for the ETL method there is intersection $t_{\min}^{\text{ETL}} = t_{\max}^{\text{ETL}}$ for the sufficiently large angles $\theta_{\text{MED}} \gtrsim 1$ and heavy mediator $m_{\text{MED}} \simeq 1$ GeV. This means that the ETL cross section dependence on θ_{MED} is more flatter in this region.

Let us estimate a typical mediator radiation angle in the analytical form for the double differential cross section. We consider the IWW approximation that implies Eq. (29), as a result, the virtual photon flux (20) does not depend on x and θ_{MED} . The simplified IWW approach allows us to estimate qualitatively θ_{MED} associated with collinear emission of the mediators.

One can write mediator radiation angle dependence of double-differential cross section as:

$$\frac{d\sigma(p + P_i \rightarrow p' + P_f + k)}{dx d\theta_{\text{MED}}} \Big|_{\text{IWW}} = C_{\sigma_{2 \rightarrow 3}^{\text{IWW}}}(x) \frac{\sin(\theta_{\text{MED}}) \left| \mathcal{A}_{l-\gamma \rightarrow l-\text{MED}}^{\text{MED}} \right|^2}{U^2(\theta_{\text{MED}})}, \quad (\text{C2})$$

where $U > 0$ variable is defined by Eq. (24)

$$C_{\sigma_{2 \rightarrow 3}^{\text{IWW}}}(x) = \frac{4\pi (c_{il}^{\text{MED}})^2 \alpha}{8\pi} \frac{\alpha \chi}{\pi} E_l^2 (1-x) \sqrt{x^2 - \frac{m_{\text{MED}}^2}{(E_l)^2}},$$

and the squared amplitude for Compton-like process

is [19]:

$$\left| \mathcal{A}_{l-\gamma \rightarrow l-\text{MED}}^{\text{MED}} \right|^2 = C_1^{\text{MED}}(x) - \frac{C_2^{\text{MED}}(x)}{U(\theta_{\text{MED}})} + \frac{C_3^{\text{MED}}(x)}{U^2(\theta_{\text{MED}})}.$$

The explicit forms of the coefficients C_i^{MED} for scalar, S, vector, V, pseudoscalar, P, and axialvector, A, types of mediator read [19, 58]:

$$\begin{aligned} C_1^S &= x^2/(1-x), & C_2^S &= 2(m_{\text{MED}}^2 - 4m_l^2)x, \\ C_3^S &= 2(m_{\text{MED}}^2 - 4m_l^2)(m_{\text{MED}}^2(1-x) + m_l^2x^2), \\ C_1^V &= 2 \frac{(2-2x+x^2)}{1-x}, & C_2^V &= 4(m_{\text{MED}}^2 + 2m_l^2)x, \\ C_3^V &= 4(m_{\text{MED}}^2 + 2m_l^2)(m_{\text{MED}}^2(1-x) + m_l^2x^2), \\ C_1^P &= x^2/(1-x), & C_2^P &= 2m_{\text{MED}}^2x, \\ C_3^P &= 2m_{\text{MED}}^2(m_{\text{MED}}^2(1-x) + m_l^2x^2), \\ C_1^A &= 4 + \left(2 + \frac{4m_l^2}{m_{\text{MED}}^2} \right) \frac{x^2}{1-x}, & C_2^A &= 4(m_{\text{MED}}^2 - 4m_l^2)x, \\ C_3^A &= 4(m_{\text{MED}}^2 - 4m_l^2)(m_{\text{MED}}^2(1-x) + m_l^2x^2). \end{aligned}$$

For the collinear singularity region $x \simeq 1$ the dominant contribution to the double-differential cross section is provided by the terms

$$\sin(\theta_{\text{MED}}) C_1^{\text{MED}}(x)/U^2(\theta_{\text{MED}})$$

for all mediators, since $C_1^{\text{MED}}(x) \propto 1/(1-x)$ in the collinear emission approach $(1-x) \ll 1$. So that, one can find typical θ_{MED} that maximizes the Eq. (C2). This condition implies that

$$\tan(\theta_{\text{typ}}^{2\text{D}}) = (1/2)U/(U)'_{\theta_{\text{MED}}}, \quad (\text{C3})$$

where $(U)'_{\theta_{\text{MED}}}$ is a derivation of (24) with respect to θ_{MED} . Finally, implying a small values $\tan(\theta_{\text{typ}}^{2\text{D}}) \simeq \theta_{\text{typ}}^{2\text{D}} \ll 1$, one can resolve aon Eq. (C3) and obtain the typical mediator radiation angle in the

following form:

$$\theta_{\text{typ}}^{2\text{D}} = \sqrt{\frac{1}{3E_l^2 x} \left(\frac{m_{\text{MED}}^2(1-x)}{x} + m_l^2 x \right)}. \quad (\text{C4})$$

In Fig. 1 we depict $\theta_{\text{typ}}^{2\text{D}}$ by black dots for various x and set of masses $m_{\text{MED}} = (5 \text{ MeV}, 1 \text{ GeV})$. Remarkably that Eq. (C4) is a fairly good estimate also for the typical angles of both ETL and WW cross sections.

Moreover, by substituting the expression for x_{min} and x_{max} into Eq. (C4), one can get the bounds on the

typical mediator radiation angle:

$$\frac{m_l}{3E_l} \left(\frac{m_l}{E_l} + \frac{m_{\text{MED}}^2}{E_l^2} \right) \lesssim (\theta_{\text{typ}}^{2\text{D}})^2 < \frac{E_l(E_l - m_{\text{MED}}) + m_l^2}{3E_l^2}.$$

Taking into account the expression above in the case of a muon beam in the region of light mediator masses, $m_{\text{MED}} \ll m_l$, we get $\frac{m_l^2}{3E_l^2} \lesssim (\theta_{\text{typ}}^{2\text{D}})^2$. Indeed, one can see from Fig. 1 that for muon beam at $m_{\text{MED}} = 0.005 \text{ GeV}$ the typical mediator radiation angles is $\theta_{\text{typ}}^{2\text{D}} \simeq m_l/(\sqrt{3}E_l)$. That implies $\theta_{\text{typ}}^{2\text{D}} \simeq 3.8 \times 10^{-4}$ and $\theta_{\text{typ}}^{2\text{D}} \simeq 4.0 \times 10^{-3}$ for NA64 μ and M³ experiments, respectively. It is also worth noting that both the cut-off and the typical mediator radiation angles of the double differential cross section scale with the energy as $\theta^{2\text{D}} \propto 1/E_l$.

-
- [1] L. Bergstrom, *Annalen Phys.* **524**, 479 (2012), [arXiv:1205.4882 \[astro-ph.HE\]](#).
- [2] G. Bertone and D. Hooper, *Rev. Mod. Phys.* **90**, 045002 (2018), [arXiv:1605.04909 \[astro-ph.CO\]](#).
- [3] M. Cirelli, A. Strumia, and J. Zupan, (2024), [arXiv:2406.01705 \[hep-ph\]](#).
- [4] G. Bertone, D. Hooper, and J. Silk, *Phys. Rept.* **405**, 279 (2005), [arXiv:hep-ph/0404175](#).
- [5] G. B. Gelmini, in *Theoretical Advanced Study Institute in Elementary Particle Physics: Journeys Through the Precision Frontier: Amplitudes for Colliders* (2015) pp. 559–616, [arXiv:1502.01320 \[hep-ph\]](#).
- [6] P. A. R. Ade *et al.* (Planck), *Astron. Astrophys.* **594**, A13 (2016), [arXiv:1502.01589 \[astro-ph.CO\]](#).
- [7] N. Aghanim *et al.* (Planck), *Astron. Astrophys.* **641**, A6 (2020), [Erratum: *Astron. Astrophys.* 652, C4 (2021)], [arXiv:1807.06209 \[astro-ph.CO\]](#).
- [8] T. Aoyama *et al.*, *Phys. Rept.* **887**, 1 (2020), [arXiv:2006.04822 \[hep-ph\]](#).
- [9] M. Davis, G. Efstathiou, C. S. Frenk, and S. D. M. White, *Astrophys. J.* **292**, 371 (1985).
- [10] B. W. Lee and S. Weinberg, *Phys. Rev. Lett.* **39**, 165 (1977).
- [11] E. W. Kolb and K. A. Olive, *Phys. Rev. D* **33**, 1202 (1986).
- [12] G. Krnjaic, *Phys. Rev. D* **94**, 073009 (2016), [arXiv:1512.04119 \[hep-ph\]](#).
- [13] J. McDonald, *Phys. Rev. D* **50**, 3637 (1994), [arXiv:hep-ph/0702143](#).
- [14] C. P. Burgess, M. Pospelov, and T. ter Veldhuis, *Nucl. Phys. B* **619**, 709 (2001), [arXiv:hep-ph/0011335](#).
- [15] J. D. Wells, , 283 (2008), [arXiv:0803.1243 \[hep-ph\]](#).
- [16] R. M. Schabinger and J. D. Wells, *Phys. Rev. D* **72**, 093007 (2005), [arXiv:hep-ph/0509209](#).
- [17] G. Bickendorf and M. Drees, *Eur. Phys. J. C* **82**, 1163 (2022), [arXiv:2206.05038 \[hep-ph\]](#).
- [18] E. E. Boos, V. E. Bunichev, and S. S. Trykov, *Phys. Rev. D* **107**, 075021 (2023), [arXiv:2205.07364 \[hep-ph\]](#).
- [19] H. Sieber, D. V. Kirpichnikov, I. V. Voronchikhin, P. Crivelli, S. N. Gninenko, M. M. Kirsanov, N. V. Krasnikov, L. Molina-Bueno, and S. K. Sekatskii, *Phys. Rev. D* **108**, 056018 (2023), [arXiv:2305.09015 \[hep-ph\]](#).
- [20] R. Catena and T. R. Gray, *JCAP* **11**, 058 (2023), [arXiv:2307.02207 \[hep-ph\]](#).
- [21] B. Holdom, *Phys. Lett. B* **166**, 196 (1986).
- [22] E. Izaguirre, G. Krnjaic, P. Schuster, and N. Toro, *Phys. Rev. Lett.* **115**, 251301 (2015), [arXiv:1505.00011 \[hep-ph\]](#).
- [23] R. Essig, P. Schuster, N. Toro, and B. Wojtsekhowski, *JHEP* **02**, 009 (2011), [arXiv:1001.2557 \[hep-ph\]](#).
- [24] Y. Kahn, G. Krnjaic, J. Thaler, and M. Toupes, *Phys. Rev. D* **91**, 055006 (2015), [arXiv:1411.1055 \[hep-ph\]](#).
- [25] B. Batell, R. Essig, and Z. Surujon, *Phys. Rev. Lett.* **113**, 171802 (2014), [arXiv:1406.2698 \[hep-ph\]](#).
- [26] E. Izaguirre, G. Krnjaic, P. Schuster, and N. Toro, *Phys. Rev. D* **88**, 114015 (2013), [arXiv:1307.6554 \[hep-ph\]](#).
- [27] A. Kachanovich, S. Kovalenko, S. Kuleshov, V. E. Lyubovitskij, and A. S. Zhevlakov, *Phys. Rev. D* **105**, 075004 (2022), [arXiv:2111.12522 \[hep-ph\]](#).
- [28] V. E. Lyubovitskij, A. S. Zhevlakov, A. Kachanovich, and S. Kuleshov, *Phys. Rev. D* **107**, 055006 (2023), [arXiv:2210.05555 \[hep-ph\]](#).
- [29] D. Gorbunov and D. Kalashnikov, *Phys. Rev. D* **107**, 015014 (2023), [arXiv:2211.06270 \[hep-ph\]](#).
- [30] J. Claude, M. Dutra, and S. Godfrey, *Phys. Rev. D* **107**, 075006 (2023), [arXiv:2208.09422 \[hep-ph\]](#).
- [31] W. Wang, W.-L. Xu, J. M. Yang, and R. Zhu, *Nucl. Phys. B* **995**, 116348 (2023), [arXiv:2305.12668 \[hep-ph\]](#).
- [32] H. M. Lee, M. Park, and V. Sanz, *Eur. Phys. J. C* **74**, 2715 (2014), [arXiv:1306.4107 \[hep-ph\]](#).
- [33] Y.-J. Kang and H. M. Lee, *Eur. Phys. J. C* **80**, 602 (2020), [arXiv:2001.04868 \[hep-ph\]](#).
- [34] N. Bernal, M. Dutra, Y. Mambrini, K. Olive, M. Peloso, and M. Pierre, *Phys. Rev. D* **97**, 115020 (2018), [arXiv:1803.01866 \[hep-ph\]](#).
- [35] M. G. Folgado, A. Donini, and N. Rius, *JHEP* **04**, 036 (2020), [arXiv:1912.02689 \[hep-ph\]](#).
- [36] Y.-J. Kang and H. M. Lee, *Eur. Phys. J. C* **81**, 868 (2021), [arXiv:2002.12779 \[hep-ph\]](#).
- [37] M. Dutra, *PoS LeptonPhoton2019*, 076 (2019), [arXiv:1911.11844 \[hep-ph\]](#).
- [38] S. Clery, Y. Mambrini, K. A. Olive, A. Shkerin, and S. Verner, *Phys. Rev. D* **105**, 095042 (2022), [arXiv:2203.02004 \[hep-ph\]](#).
- [39] J. A. Gill, D. Sengupta, and A. G. Williams, *Phys. Rev.*

- D** **108**, L051702 (2023), arXiv:2303.04329 [hep-ph].
- [40] W. Wang, L. Wu, J. M. Yang, H. Zhou, and B. Zhu, *JHEP* **12**, 072 (2020), [Erratum: *JHEP* **02**, 052 (2021)], arXiv:1912.09904 [hep-ph].
- [41] A. de Giorgi and S. Vogl, *JHEP* **11**, 036 (2021), arXiv:2105.06794 [hep-ph].
- [42] A. de Giorgi and S. Vogl, *JHEP* **04**, 032 (2023), arXiv:2208.03153 [hep-ph].
- [43] K. Jodłowski, *Phys. Rev. D* **108**, 115017 (2023), arXiv:2305.05710 [hep-ph].
- [44] S. N. Gninenko, N. V. Krasnikov, M. M. Kirsanov, and D. V. Kirpichnikov, *Phys. Rev. D* **94**, 095025 (2016), arXiv:1604.08432 [hep-ph].
- [45] D. Banerjee *et al.* (NA64), *Phys. Rev. Lett.* **118**, 011802 (2017), arXiv:1610.02988 [hep-ex].
- [46] D. Banerjee *et al.* (NA64), *Phys. Rev. D* **97**, 072002 (2018), arXiv:1710.00971 [hep-ex].
- [47] S. N. Gninenko, D. V. Kirpichnikov, and N. V. Krasnikov, *Phys. Rev. D* **100**, 035003 (2019), arXiv:1810.06856 [hep-ph].
- [48] D. Banerjee *et al.*, *Phys. Rev. Lett.* **123**, 121801 (2019), arXiv:1906.00176 [hep-ex].
- [49] R. R. Dusaev, D. V. Kirpichnikov, and M. M. Kirsanov, *Phys. Rev. D* **102**, 055018 (2020), arXiv:2004.04469 [hep-ph].
- [50] Y. M. Andreev *et al.*, *Phys. Rev. D* **104**, L091701 (2021), arXiv:2108.04195 [hep-ex].
- [51] Y. M. Andreev *et al.* (NA64), *Phys. Rev. Lett.* **129**, 161801 (2022), arXiv:2207.09979 [hep-ex].
- [52] Y. M. Andreev *et al.* (NA64), *Phys. Rev. D* **106**, 032015 (2022), arXiv:2206.03101 [hep-ex].
- [53] N. Arefyeva, S. Gninenko, D. Gorbunov, and D. Kirpichnikov, *Phys. Rev. D* **106**, 035029 (2022), arXiv:2204.03984 [hep-ph].
- [54] A. S. Zhevlakov, D. V. Kirpichnikov, and V. E. Lyubovitskij, *Phys. Rev. D* **106**, 035018 (2022), arXiv:2204.09978 [hep-ph].
- [55] C. Cazzaniga *et al.* (NA64), *Eur. Phys. J. C* **81**, 959 (2021), arXiv:2107.02021 [hep-ex].
- [56] Y. M. Andreev *et al.* (NA64), *Phys. Rev. Lett.* **126**, 211802 (2021), arXiv:2102.01885 [hep-ex].
- [57] H. Sieber, D. Banerjee, P. Crivelli, E. Depero, S. N. Gninenko, D. V. Kirpichnikov, M. M. Kirsanov, V. Poliakov, and L. Molina Bueno, *Phys. Rev. D* **105**, 052006 (2022), arXiv:2110.15111 [hep-ex].
- [58] D. V. Kirpichnikov, H. Sieber, L. M. Bueno, P. Crivelli, and M. M. Kirsanov, *Phys. Rev. D* **104**, 076012 (2021), arXiv:2107.13297 [hep-ph].
- [59] Y. M. Andreev *et al.* (NA64), *Phys. Rev. Lett.* **132**, 211803 (2024), arXiv:2401.01708 [hep-ex].
- [60] A. Berlin, N. Blinov, G. Krnjaic, P. Schuster, and N. Toro, *Phys. Rev. D* **99**, 075001 (2019), arXiv:1807.01730 [hep-ph].
- [61] A. M. Ankowski, A. Friedland, S. W. Li, O. Moreno, P. Schuster, N. Toro, and N. Tran, *Phys. Rev. D* **101**, 053004 (2020), arXiv:1912.06140 [hep-ph].
- [62] P. Schuster, N. Toro, and K. Zhou, *Phys. Rev. D* **105**, 035036 (2022), arXiv:2112.02104 [hep-ph].
- [63] T. Åkesson *et al.*, in *Snowmass 2021* (2022) arXiv:2203.08192 [hep-ex].
- [64] R. Capdevilla, D. Curtin, Y. Kahn, and G. Krnjaic, *JHEP* **04**, 129 (2022), arXiv:2112.08377 [hep-ph].
- [65] Y. Kahn, G. Krnjaic, N. Tran, and A. Whitbeck, *JHEP* **09**, 153 (2018), arXiv:1804.03144 [hep-ph].
- [66] E. Fermi, *Nuovo Cim.* **2**, 143 (1925), arXiv:hep-th/0205086.
- [67] C. F. von Weizsacker, *Z. Phys.* **88**, 612 (1934).
- [68] E. J. Williams, *Kong. Dan. Vid. Sel. Mat. Fys. Med.* **13N4**, 1 (1935).
- [69] K. J. Kim and Y.-S. Tsai, *Phys. Rev. D* **8**, 3109 (1973).
- [70] Y.-S. Tsai, *Rev. Mod. Phys.* **46**, 815 (1974).
- [71] V. M. Budnev, I. F. Ginzburg, G. V. Meledin, and V. G. Serbo, *Phys. Rept.* **15**, 181 (1975).
- [72] Y.-S. Liu, D. McKeen, and G. A. Miller, *Phys. Rev. D* **95**, 036010 (2017), arXiv:1609.06781 [hep-ph].
- [73] Y.-S. Liu and G. A. Miller, *Phys. Rev. D* **96**, 016004 (2017), arXiv:1705.01633 [hep-ph].
- [74] J. Blümlein and J. Brunner, *Phys. Lett. B* **731**, 320 (2014), arXiv:1311.3870 [hep-ph].
- [75] S. Foroughi-Abari and A. Ritz, *Phys. Rev. D* **105**, 095045 (2022), arXiv:2108.05900 [hep-ph].
- [76] S. Foroughi-Abari, P. Reimitz, and A. Ritz, (2024), arXiv:2409.09123 [hep-ph].
- [77] D. Gorbunov and E. Kriukova, *JHEP* **01**, 058 (2024), arXiv:2306.15800 [hep-ph].
- [78] L. Harland-Lang, J. Jaeckel, and M. Spannowsky, *Phys. Lett. B* **793**, 281 (2019), arXiv:1902.04878 [hep-ph].
- [79] D. Gorbunov and E. Kriukova, (2024), arXiv:2409.11386 [hep-ph].
- [80] D. Gorbunov and E. Kriukova (2024) arXiv:2409.11089 [hep-ph].
- [81] We recall that ETL method implies the straightforward cross section calculation without exploiting any simplification approaches.
- [82] D. Forbes, C. Herwig, Y. Kahn, G. Krnjaic, C. Mantilla Suarez, N. Tran, and A. Whitbeck, *Phys. Rev. D* **107**, 116026 (2023), arXiv:2212.00033 [hep-ph].
- [83] G. Krnjaic, D. Rocha, and I. R. Wang, (2024), arXiv:2409.00170 [hep-ph].
- [84] H. Davoudiasl, R. Marcarelli, and E. T. Neil, *JHEP* **02**, 071 (2023), arXiv:2112.04513 [hep-ph].
- [85] B. Batell, H. Davoudiasl, R. Marcarelli, E. T. Neil, and S. Trojanowski, *Phys. Rev. D* **110**, 075039 (2024), arXiv:2407.15942 [hep-ph].
- [86] A. Ponten, H. Sieber, B. B. Oberhauser, P. Crivelli, D. Kirpichnikov, S. N. Gninenko, M. Hösken, L. M. Bueno, M. Mongillo, and A. Zhevlakov, *Eur. Phys. J. C* **84**, 1035 (2024), arXiv:2404.15931 [hep-ph].
- [87] H. Davoudiasl, R. Marcarelli, and E. T. Neil, *Phys. Rev. D* **108**, 075017 (2023), arXiv:2307.00102 [hep-ph].
- [88] K. Asai, S. Iwamoto, Y. Sakaki, and D. Ueda, *JHEP* **09**, 183 (2021), arXiv:2105.13768 [hep-ph].
- [89] K. Asai, S. Iwamoto, M. Perelstein, Y. Sakaki, and D. Ueda, *JHEP* **02**, 129 (2024), arXiv:2301.03816 [hep-ph].
- [90] T. Araki, K. Asai, and T. Shimomura, *JHEP* **11**, 082 (2021), arXiv:2107.07487 [hep-ph].
- [91] K. Asai, A. Das, J. Li, T. Nomura, and O. Seto, *Phys. Rev. D* **106**, 095033 (2022), arXiv:2206.12676 [hep-ph].
- [92] J. Liu, Y. Luo, and M. Song, *JHEP* **09**, 104 (2023), arXiv:2304.05435 [hep-ph].
- [93] A. S. Zhevlakov, D. V. Kirpichnikov, and V. E. Lyubovitskij, *Phys. Rev. D* **109**, 015015 (2024), arXiv:2307.10771 [hep-ph].
- [94] J. Liang, Z. Liu, and L. Yang, *JHEP* **05**, 273 (2024), arXiv:2212.04252 [hep-ph].
- [95] J. Liang, Z. Liu, and L. Yang, *JHEP* **05**, 184 (2022), arXiv:2111.15533 [hep-ph].

- [96] T. Moroi and A. Niki, *JHEP* **05**, 016 (2023), [arXiv:2205.11766 \[hep-ph\]](#).
- [97] C. Cesarotti and R. Gambhir, *JHEP* **05**, 283 (2024), [arXiv:2310.16110 \[hep-ph\]](#).
- [98] P. Fayet and M. O. Olea-Romacho, *JHEP* **07**, 223 (2024), [arXiv:2405.02104 \[hep-ph\]](#).
- [99] C. Rella, B. Döbrich, and T.-T. Yu, *Phys. Rev. D* **106**, 035023 (2022), [arXiv:2205.09870 \[hep-ph\]](#).
- [100] B. Radics, L. Molina-Bueno, L. Fields., H. Sieber, and P. Crivelli, *Eur. Phys. J. C* **83**, 775 (2023), [arXiv:2306.07405 \[hep-ex\]](#).
- [101] S. N. Gninenko, D. V. Kirpichnikov, M. M. Kirsanov, and N. V. Krasnikov, *Phys. Lett. B* **782**, 406 (2018), [arXiv:1712.05706 \[hep-ph\]](#).
- [102] J. D. Bjorken, R. Essig, P. Schuster, and N. Toro, *Phys. Rev. D* **80**, 075018 (2009), [arXiv:0906.0580](#).
- [103] B. Batell, A. Freitas, A. Ismail, and D. Mckeen, *Phys. Rev. D* **98**, 055026 (2018), [arXiv:1712.10022 \[hep-ph\]](#).
- [104] C.-Y. Chen, J. Kozaczuk, and Y.-M. Zhong, *JHEP* **10**, 154 (2018), [arXiv:1807.03790 \[hep-ph\]](#).
- [105] L. Marsicano, M. Battaglieri, A. Celentano, R. De Vita, and Y.-M. Zhong, *Phys. Rev. D* **98**, 115022 (2018), [arXiv:1812.03829 \[hep-ex\]](#).
- [106] J. Mans (LDMX), *EPJ Web Conf.* **142**, 01020 (2017).
- [107] T. Åkesson *et al.* (LDMX), (2018), [arXiv:1808.05219 \[hep-ex\]](#).
- [108] M. D. Schwartz, *Quantum Field Theory and the Standard Model* (Cambridge University Press, 2014).
- [109] S. D. Drell and J. D. Walecka, *Annals Phys.* **28**, 18 (1964).
- [110] V. B. Berestetskii, E. M. Lifshitz, and L. P. Pitaevskii, *QUANTUM ELECTRODYNAMICS*, Course of Theoretical Physics, Vol. 4 (Pergamon Press, Oxford, 1982).
- [111] T. Beranek, H. Merkel, and M. Vanderhaeghen, *Phys. Rev. D* **88**, 015032 (2013), [arXiv:1303.2540 \[hep-ph\]](#).
- [112] M. P. Rekaló and E. Tomasi-Gustafsson, (2002), [arXiv:nucl-th/0202025](#).
- [113] C. F. Perdrisat, V. Punjabi, and M. Vanderhaeghen, *Prog. Part. Nucl. Phys.* **59**, 694 (2007), [arXiv:hep-ph/0612014](#).
- [114] L. I. Schiff, *Phys. Rev.* **83**, 252 (1951).
- [115] L. I. Schiff, *Phys. Rev.* **92**, 988 (1953), [Erratum: *Phys. Rev.* 93, 1434–1434 (1954)].
- [116] J. D. Lewin and P. F. Smith, *Astropart. Phys.* **6**, 87 (1996).
- [117] B. Döbrich, J. Jaeckel, F. Kahlhoefer, A. Ringwald, and K. Schmidt-Hoberg, *JHEP* **02**, 018 (2016), [arXiv:1512.03069 \[hep-ph\]](#).
- [118] K. Freese, J. A. Frieman, and A. Gould, *Phys. Rev. D* **37**, 3388 (1988).
- [119] C.-Y. Chen, M. Pospelov, and Y.-M. Zhong, *Phys. Rev. D* **95**, 115005 (2017), [arXiv:1701.07437 \[hep-ph\]](#).
- [120] V. Shtabovenko, R. Mertig, and F. Orellana, *Comput. Phys. Commun.* **256**, 107478 (2020), [arXiv:2001.04407 \[hep-ph\]](#).
- [121] V. Shtabovenko, R. Mertig, and F. Orellana, *Comput. Phys. Commun.* **207**, 432 (2016), [arXiv:1601.01167 \[hep-ph\]](#).
- [122] W. R. Inc., “Mathematica, Version 13.1,” Champaign, IL, 2022.
- [123] M. Bondi, A. Celentano, R. R. Dusaev, D. V. Kirpichnikov, M. M. Kirsanov, N. V. Krasnikov, L. Marsicano, and D. Shchukin, *Comput. Phys. Commun.* **269**, 108129 (2021), [arXiv:2101.12192 \[hep-ph\]](#).
- [124] B. B. Oberhauser *et al.*, *Comput. Phys. Commun.* **300**, 109199 (2024), [arXiv:2401.12573 \[hep-ph\]](#).
- [125] Y. M. Andreev *et al.* (NA64), *Phys. Rev. D* **110**, 112015 (2024), [arXiv:2409.10128 \[hep-ex\]](#).
- [126] I. V. Voronchikhin and D. V. Kirpichnikov, *Phys. Rev. D* **109**, 075012 (2024), [arXiv:2312.15697 \[hep-ph\]](#).
- [127] I. Voronchikhin, “High energy physics and dark sector,” (2025), gitHub repository.